MAXIMUM POWER POINT TRACKING USING MRAC FOR A SOLAR POWER GENERATION SYSTEM

MSC THESIS

LEGESSE DESTA KEIMISSO

HAWASSA UNIVERSITY, HAWASSA, ETHIOPIA

JULY,2020

MAXIMUM POWER POINT TRACKING USING MRAC FOR A SOLAR POWER GENERATION SYSTEM

LEGESSE DESTA KEIMISSO

A THESIS SUBMITTED TO THE
FACULTY OF ELECTRICAL ENGINEERING
DEPARTMENT OF ELECTRICAL AND COMPUTER ENGINEERING
SCHOOL OF GRADUATE STUDIES
HAWASSA UNIVERSITY, HAWASSA, ETHIOPIA

IN PARTIAL FULFILLMENT OF THE
REQUIREMENTS FOR THE DEGREE OF

MASTER OF SCIENCE IN
ELECTRICAL AND COMPUTER ENGINEERING
(SPECIALIZATION: CONTROL AND INSTRUMENTATION ENGINEERING)

JULY, 2020

ADVISORS' APPROVAL SHEET

This is to certify that the thesis entitled "**Maximum Power Point Tracking Using MRAC For A Solar Power Generation System"** submitted in partial fulfillment of the requirements for the degree of Master's in control and instrumentation Engineering, the Graduate Program of the Department of Electrical and Computer Engineering, and has been carried out by Legesse Desta ID. No: PGCon/026/09, under my supervision. Therefore, I recommend that the student has fulfilled the requirements and hence hereby can submit the thesis to the department.

Gebremichael Te-ame (Dr-Ing)	_____	_____
Name of Major Advisor	Signature	Date

EXAMINERS' APPROVAL SHEET

We, the undersigned members of the Board of Examiners of the final open defense by Legesse Desta, have read and evaluated his thesis entitled "**Maximum Power Point Tracking Using MRAC For A Solar Power Generation System**", and examined the candidate. This is, therefore, to certify that the thesis has been accepted in partial fulfillment of the requirements for the degree.

Mr. Muluken Regassa	_____	_____
Name of the Chairperson	Signature	Date
Dr.-Ing Gebremichael Te-ame	_____	_____
Name of Major Advisor	Signature	Date
Mr. Yeshitla Hailu	_____	_____
Name of Internal Examiner	Signature	Date
Dr. Beteley Teka	_____	_____
Name of External examiner	Signature	Date
_____.	_____	_____
SGS Approval	Signature	Date

DECLARATION

I hereby declare that this Msc thesis entitled "**Maximum Power Point Tracking Using MRAC For a Solar Power Generation System**" is my original work and has not been presented for a degree in any other university, and all sources of material used for this thesis have been duly acknowledged.

Name Signature

Legesse Desta _____

This Msc thesis entitled "**Maximum Power Point Tracking Using MRAC For a Solar Power Generation System**" has been submitted for examination with my approval as thesis advisor.

Gebremichael Te-ame (Dr-Ing) _____ _____

Advisor's Name Signature Date

Place:_____

Date of submission**:** _____

ACKNOWLEDGMENTS

First of all, I would like to express my greatest gratitude to God; success is impossible without him.

Secondly, I would like to express my deepest gratitude to my advisor Dr.-Ing. Gebremichael Te-ame for his wonderful guidance, constructive comments, suggestions, and encouragement during the overall process of this thesis.

Last but not least, I would like to express my heartiest appreciation to my family and my friends for their encouragement, cooperation, and support.

ABSTRACT

The sun is the most abundant and sustainable source of energy. A large amount of energy reaches the surface of the earth from the sun, but from this energy small portion would be sufficient to assure the global estimated power demand. To effectively assure this power demand we are facing different problems to develop the efficient ways to extract, transform, accumulate, and use this available energy at reasonable costs. Many types of research were done to increase the efficiency of extracting maximum power from solar irradiations either mechanically or electrically. Mechanically like using sun-tracking and concentrating solar thermal systems to use solar energy as a source of heat for conventional power generation. Electrically by using Maximum Power Point Tracking (MPPT) algorithms. However, there is a problem associated with these MPPT techniques, which is unwanted oscillation near the maximum power point. In this thesis, the model reference adaptive controller was designed to reduce this unwanted oscillation. To design the proposed controller, model reference adaptive controller, the Lyapunov approach was applied. The proposed controller has been tested and validated using Matlab simulation for various irradiation levels. Finally, we found that the model reference adaptive controller improves settling time and reduces an oscillation in maximum power point.

***Keywords**: Duty cycle, Lyapunov rule, MPPT, MRAC, PV Cell, RCC*

TABLE OF CONTENTS

LIST OF ABBREVIATIONS

Ego Band gap energy of semiconductors

G Irradiation

Io Saturation current of PV module

Isc Short circuit current of PV module

Iph Photo current

Ipv Photovoltaic current

K Boltzman constant

Ki Short circuit current temperature constant

MPPT Maximum Power Point Tracking

MRAC Model Reference Adaptive Control

Ns Number of cells connected in series

Np Number of cells connected in parallel

OCV Open Circuit Voltage

P & O Perturb and Observe

PV Photovoltaic

q Electron charge

RCC Ripple Correlation Control

SSC Short Circuit Current

SMPS Switching Mode Power supply

LIST OF TABLES

LIST OF FIGURES

CHAPTER ONE
INTRODUCTION

1.1 Background

Utilizing energy that is obtained from sustainable sources, like the sun, became an interesting area during the 17th century following the oil crisis. During that era, the economic questions were the vital issue and the concern for sustainable energy was decreased when the cost of an oil fell. Currently, the high concern is given to utilize renewable energies, due to the need for minimizing the high environmental pollution emitted by the fossil energy system. Sun is a plentiful and renewable energy source, which produces beyond 150,000 terawatts of power to the Earth; from this energy around 50%, falls on the Earth surface but the remaining amount returned to space. From the energy falls on the earth's surface small portion could be sufficient to assure the world estimated power demand. The problems we are facing in generating energy from the PV system is to develop effective methods to extract, transform, accumulate, and use this available energy at a reasonable cost [1].

Green energy refers to renewable, clean, and environmentally friend energy sources. Solar based and wind-based power generating systems are feasible solutions for villages that are not connected to the national electric grid. Utilizing sustainable energy sources mainly depends on three basic factors that are, accessibility, affordability, and acceptability [2].

The two key problems of photovoltaic energy:

a) The cost is expensive and

b) It is not perpetually accessible once it is required.

Extensive researches were done to develop methods, which possibly will support to conquer these key problems. Designing an appropriate controller is one of those techniques. Nowadays, the conventional power source is decreasing, then exploration into a renewable energy source is becoming an interesting and significant area. The U.S. Department of Energy plans to get 20% of its power supply from sustainable sources in 2030. This is more than three hundred thousand megawatts of power. Currently, in Europe, wind power plants have been built in offshore of Denmark. The structure of power systems should be changed, consequently due to an increase in the utilization of renewable energy sources. Hence, sophisticated control algorithms are required for solving the problems that happen in renewable energy. Nowadays, the grid system is becoming advanced. This advancement aims to make the grid system highly robust and smarter to reduce instability in voltage and power [3]. Wind and solar energies are interesting energy

sources, mainly because of the availability of the resource, the cost, and environmental issues. Indications such as government policies, installation of huge photovoltaic based power generation systems, and producing a large number of solar panels lead us to conclude that the solar energy may become the leading source of energy for the next generation. Nowadays, the conversion efficiency of photovoltaic energy to electrical energy is about 12-22%. To enhance the conversion efficiency considerably; it needs the upgrading of available photon material to convert photovoltaic to electrical energy in an effective manner [4].

1.2 Statement of the Problem

Some fraction of the solar energy fall on the Earth's surface would be sufficient to assure the global energy demand. One of the problems we are experiencing in solar power generation is to design an effective strategy to extract, transform, accumulate, and use this energy at a reasonable cost. Solar irradiation, which is the main source of power in the solar energy system, cannot be controlled, and it varies daily and seasonally in an irregular manner. However, the fuel, which is the major source of power, can be controlled in other power generating systems. So, these variations in environmental conditions will bring diverse power values. To increase the efficiency of the overall system, PVS always needs to work in its maximum power point (MPP) to deliver the maximum amount of power to the load. Hence; an algorithm that can regulate this power change is needed. Most MPPT algorithms were unable to attain the MPP without an oscillation. Therefore, there is a need to develop an advanced controller that accommodates these nonlinear characteristics and improves the efficiency of tracking MPP for the solar-based energy generation system.

1.3 Objectives

1.3.1. The general objective

The main objective of the thesis is to design the MPPT controller by using the Model reference adaptive controller for optimizing the power generated by the Photovoltaic based power system.

1.3.2 Specific objective

The specific objectives that result in the general objective are:-

- To develop the model of the Photovoltaic system.
- To design a control algorithm for Maximum power tracking of the photovoltaic based power system.

- To design model Reference Adaptive control (MRAC) for PV based solar power system.
- To test the performance analysis and compare it with some benchmark controller.
- To validate the results.

1.4 Methodology

To meet the above-specified objectives, there are a couple of steps that shall be followed in doing the thesis work. The first step includes the review and study of various kinds of related literature which help to understand the necessary theoretical background for research work and helps to understand and identify the problems. To revise the literature, various published journals and books were used as the source of data. In the second step, System Modeling was carried out. In the third step a mathematical model, showing all the system dynamics with the necessary steps was derived. Both controllers, RCC and MRAC were designed using inherent ripples and Lyapunov stability theorem respectively. Finally, based on simulation results the system performance was tested and the results were validated.

1.5 Scope and limitations.

The thesis focuses on the design of a model reference adaptive controller for optimizing the power generated by a Photovoltaic based solar power system. The MPPT algorithm was designed to find an operating point for maximum power. It is mainly functional to the unimodal system means the system that has only one extreme point, and its objective is finding the maximum point of a system. A solar panel also possesses multimodal characteristics that bring other potential challenges like multiple extreme points. This thesis focuses only on the unimodal characteristics of the solar panel.

No real implementation was done for the proposed control system. Testing its effectiveness was limited to Matlab Simulink simulation. For simulation, no real solar radiation was used instead, the signal builder was used to generate a signal as solar irradiation.

1.6 Thesis Organization

The remaining part of the thesis work is organized in the following manner. Chapter two contains the literature review. Chapter three focuses on mathematical modeling. Chapter four shows the controller design. Chapter five deals with simulation results and discussions. Finally, chapter six focuses on conclusions, recommendations, and future work.

CHAPTER TWO
LITERATURE REVIEW

2.1 Overview

This chapter covers the theoretical background of solar panel, DC-DC boost converter, maximum power point tracking algorithms and the model reference adaptive controller. Different articles and journals were reviewed that have been done so far related to the solar power generation system.

2.2 Theoretical Background of a solar panel

A photovoltaic (PV) system directly converts sunlight into electricity [5]. A Photovoltaic cell is a semiconductor wafer, that is built by using two layers typically from pure silicon. The layers may be doped with boron and phosphorous one on either side, to produce an excess of electrons and deficient of electrons on the other side. When light from solar irradiation hits this semiconductor wafer, the surplus of electrons will be released. This creates a potential difference among the two sides, then the surplus of electrons will shift to the shortage side. Silicon has a voltage difference of 0.5 volts. When an external circuit coupled to the metallic contacts of the semiconductor wafer, the electrons start to move through an externally connected circuit, and then the current starts to flow. A PV array made up of several PV cells, which can be connected either in parallel or in a series to increase current and voltage respectively [6].

The PV cell is a basic device of a PV system. When cells grouped they form panels or arrays. The voltage and current, that are available at the terminals of a PV device may directly feed small loads such as lighting systems, DC motors, and converters which may or may not be connected to load or grid. More sophisticated applications need electronic converters to process the electric power from the PV panel. These converters were useful to regulate the current and voltage at the load, to control the power flow in grid-connected systems, and mainly to track the maximum power point (MPP) of the system. To study about the converters of the PV systems, one initially should have to be familiar with the way to model the PV panel that is coupled to the converter. PV device I-V and P-V characteristic to various panels' combination, temperature, and radiation is shown in figure 2.1 below.

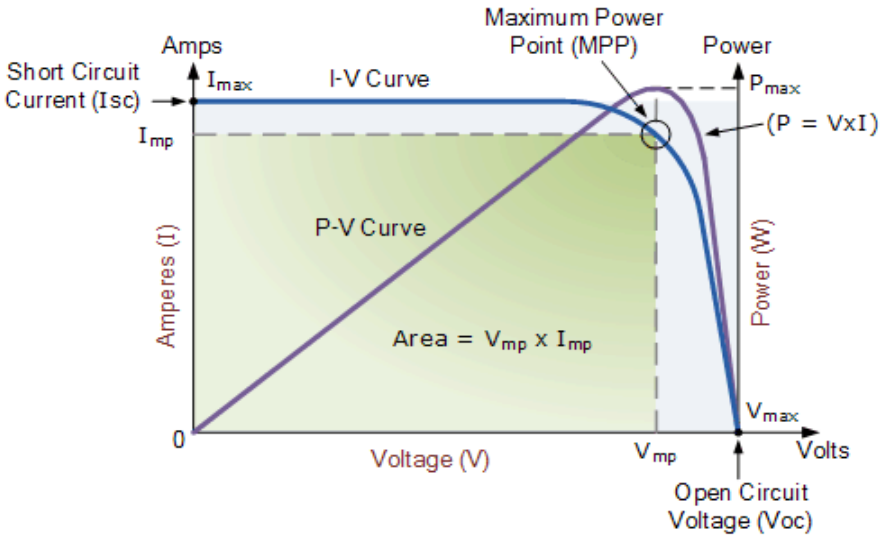

Figure 2.1: The current-voltage (I-V) characteristics of a typical silicon PV cell operating under normal conditions [6].

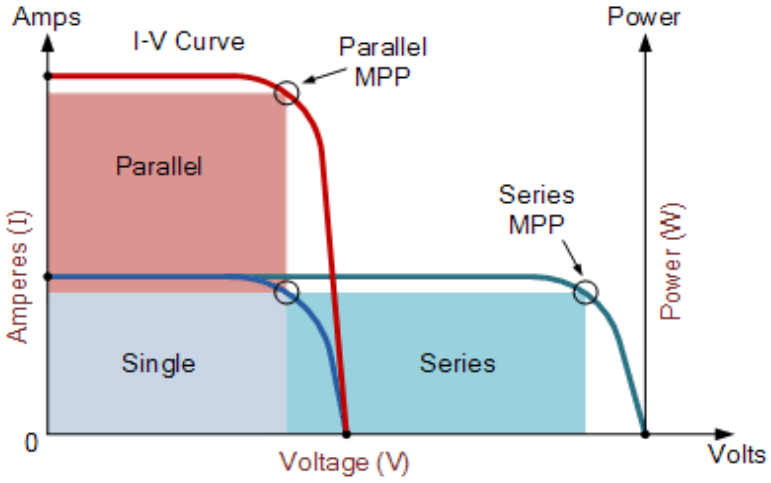

Figure2.2: Photovoltaic panels wired or connected in either series or parallel combinations [6]

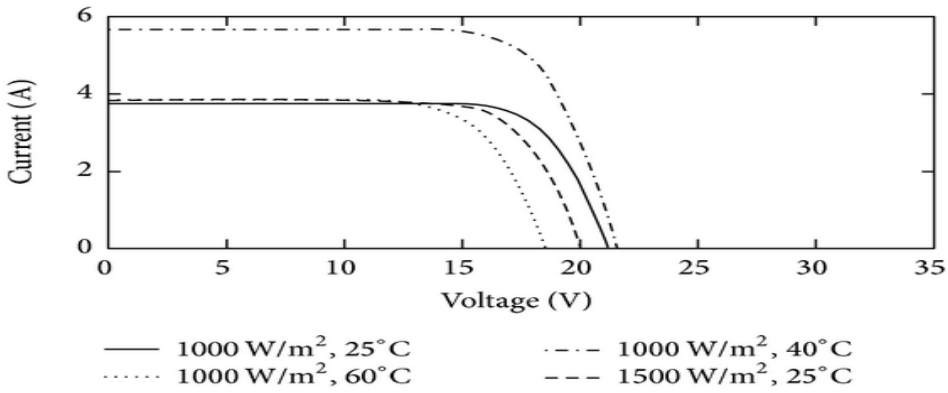

Figure 2.3: I-V characteristics of photovoltaic systems under various levels of solar irradiation and temperature [7].

2.3 DC-DC boost converter

DC-DC boost converter converts a fluctuating input dc voltage into an increased and stable output dc voltage. These converters consist of elements such as MOSFETS, transistors, and diodes to function a binary switching. They also consist of inductive and capacitive components used to remove noise, accumulate, and transmit energy. The DC-DC boost converter is used to provide maximum power to the load. The MPPT algorithm is used to regulate the DC-DC converter to make the output voltage of the PV module to be maintained at its maximum point. Solar irradiation varies radically before it reaches on the surface of a PV array due to environmental variations such as mugginess and cloud cover. Solar Irradiation changes more rapidly as compared to variation in temperature. Due to this factor, the MPPT algorithm should be developed based on the rapid dynamics of solar irradiation to mitigate the delay and tracking error of the MPP. MPPT requires the dc-dc converter in between photovoltaic array and load to retain the PV array output voltage or current at the maximum for a certain level of solar irradiation and temperature by regulating the duty cycle of converter [8]. Based on maximum power transfer theory, maximum power is being transmitted from a source to load when the load matching principle is satisfied, where the impedance at a source and the impedance at the load side must be equal. It can be achieved by regulating the duty cycle of the converter. For MPPT the converter needs to be operated with duty cycle corresponding to maximum power at a specific temperature and solar irradiation. With changing environmental conditions the duty cycle of the converter should be attuned to get optimum power from PV array [9].

2.4 Maximum Power Point Tracking (MPPT) Algorithm

PV array shows non-linear I-V characteristics and output power depends on atmospheric conditions such as solar irradiation and environmental temperature. I-V and P-V characteristic curve of PV array shows the MPP, which indicates the maximum array output power. The position of the MPP varies with variation in environmental conditions. The main function of MPPT is to regulate the photovoltaic system operating voltage near to its maximum under variable solar irradiance and temperature. To extract the maximum power from the PV array regularly, the array must operate at their maximum power point, even if there is non-uniform variation in solar irradiation and temperature. Depending on these two parameters, temperature and solar irradiation there is a distinctive maximum point in the P-V characteristics curve. The use of a maximum power point tracking algorithm (MPPT) is continuously enabling the PV array to function at the nominal value. Therefore, output power can be maintained at its maximum value [10, 11, 12].

Several MPPT algorithms have been reported in the literature. In this section, the most frequently used methods are described. From these methods, Incremental Conductance and Perturb and Observe are popular [10].

Incremental Conductance and Perturb and Observe methods are established on the principle called “hill-climbing” means adjusting the PV array operating point in the way to increase power. Hill-climbing methods are the well-known MPPT approaches due to their better performance and their simplicity to implement during unvarying solar irradiation. They also require a straightforward computational power. Their drawbacks are oscillations at MPP and they lose MPP tracking efficiency for fast varying environmental conditions [10, 12].

2.4.1 Perturb and observe

Perturb and Observe method works periodically perturbing the PV array output voltage by using an external signal. During this perturbation, the array output voltage or array output current can be either increased or decreased, and the PV output power can be compared for each perturbation cycle. If the operating voltage of the array increases, then the array power also increases ($dP_{Pv}/dV_{PV} > 0$). Therefore, the control system shifts the PV array operating point in the same direction unless in the reverse direction. The algorithm will continue similarly until the desired operating point of the system is attained [12]. P&O is an iterative method, which senses the solar panel output voltage periodically and compares the PV panel output power with that of the preceding power; the difference in power (ΔP_{PV}) is calculated. If the change in power (ΔP_{PV}) is positive, the perturbation of the array voltage should be in the similar direction of the increment. Nevertheless, if ΔP_{PV} is less than zero, the PV array operating point is away from the maximum point and during this time to return the operating point of the system towards the MPP, the perturbation should be in the reverse way of the increment The process ends when $dP_{PV}/dV_{PV}=0$ irrespective of the solar irradiation and PV module's terminal voltage [11, 13].

A common drawback of the P&O method is that the perturbation of array voltage is done in each maximum power tracking cycle. This results in an oscillation around the MPP and this oscillation causes power loss. Moreover, the P&O method can fail to track the MPP in fast varying environmental conditions. This method uses an external signal and circuitry to perturb the current position of solar array operating point to attain the MPP [11, 12, 14].

2.4.2 Incremental Conductance Methods

This method is based on the slope of the characteristics curve of the PV module. It relates the slope of the PV output power with the output voltage in the following procedure to determine the MPP.

- $\Delta P/\Delta V = 0$ at the MPP
- $\Delta P/\Delta V > 0$ on the left
- $\Delta P/\Delta V < 0$ on the right

This method has two main disadvantages, such as if the irradiation fluctuates rapidly it will lose tracking the MPP and the oscillations of the voltage and current about the MPP in the steady-state [10].

2.4.3 Open Circuit Voltage (OCV)

This method is one of the techniques of MPPT, which based on the principle that the ratio between the PV array open-circuit voltage and maximum output voltage is constant k.

$$Voc/\mathrm{Vmpp} \approx k \approx 0.76$$

Many researchers suggested good values for k found in the range of 0.7–0.80 [15].

2.4.4 Constant Voltage (CV)

This method is easiest of all maximum power tracking techniques with rapid control action. This technique does not need extra circuit or input excluding the measurement of the array output voltage. This technique needs a PI controller to adjust the converter duty ratio to keep the array output voltage around maximum point by relating the array output voltage with a reference voltage value (Vref). The value of reference voltage is obtained from the measuring the array maximum output voltage at standard test conditions (STC) or adjusted to a constant value [15].

2.4.5 Short Circuit Current (SCC)

This method is based on the principle that the PV module short circuit current and the PV module maximum output current at MPP are linearly proportional. The error between the two currents is applied to control the duty cycle of the converter. It can be related as follows

$$\mathrm{Impp} \approx K * \mathrm{Isc}$$

Where K is a constant; its estimated value by different authors is between 0.78-0.92. The two techniques, open-circuit voltage, and short circuit current were easier to implement by analog software. Their disadvantage is poor to track the MPP when compared to other methods [15].

2.4.6 Ripple Correlation control

The latest algorithm known as RCC tracks the MPP without external perturbations at each sampling time. In a place of external perturbation, it uses the advantage of using inherently incorporated ripples that exist in the array output voltage, current, and power signals produced during switching of the converter. This algorithm correlates the two parameters, variable output power and the variable output voltage or current of the photovoltaic array. If the PV module output voltage or current increases and the power also increases, then during this time the derivatives of power and current or voltage are both greater than zero, and the product of their time derivative is also positive. This shows that the current operating point is on the left side of the maximum power point. To shift the operating point towards the maximum power point the module voltage required to be incremented or the duty ratio required to be reduced, and if the current operating point lies on the right side of the maximum power point, then to shift the operating point towards maximum power point the module voltage required to be reduced or the duty ratio required to be incremented. To attain steady-state $\mathrm{dp/di} = 0$ with integral feedback control, the duty ratio D can be calculated based on the law $\mathrm{D} = \mathrm{k}\int(\mathrm{dp/di})\mathrm{dt}$. Conversely, applying a direct derivative of power with the respect to current is challenging to apply in real circuits. Due to this challenge an alternative control method can be $\mathrm{D} = \mathrm{k}\int(\mathrm{dp/dt})(\mathrm{di/dt})\,\mathrm{dt}$. The key benefit we get while using RCC over other algorithms is obtaining inherent ripples, which is produced during switching, in the converter as an alternative of using external signals for perturbation. The algorithm asymptotically converges rapidly towards MPP [13, 14, 16].

2.4.7 Model Reference Adaptive Control

To adapt means to vary a behavior to learn a new situation. Generally, adaptive control is thus, a controller that adjusts its behavior based on response for changes in the controlled plant and other disturbances. An adaptive controller is a type controller that has a parameter adjustment mechanism. It has two loops, the first one is the ordinary feedback loop consists of process/plant and controller, and the second one is parameter adjustment mechanism loop which is not faster than the ordinary feedback loop [17].

Model Reference Adaptive Control, or MRAC, is a type of control system which contains the reference model and a plant to be controlled. The required performance is specified in terms of a reference model that produces the desired response to a command signal. The command signal produced by MRAC is given as an input to both the reference model and the actual system. Then the controller starts to adapt the gains this results in minimization of output error and the

controlled plant/process reacts like the desired or model plant/process [18].The block diagram for this structure is shown in Figure 2.4.

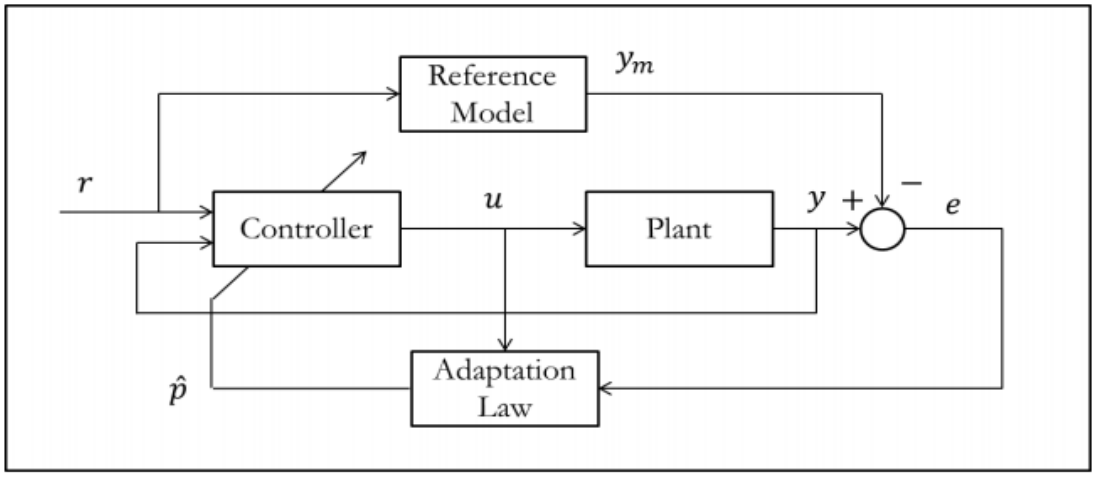

Figure 2.4: A model reference adaptive control structure [19].

2.5 Review of other related works

In [1] model predictive control of Solar Energy System was proposed. The method used mirrors, and solar tracking systems to collect and concentrate sunlight from a wide area into a smaller receiving area. The concentrated sunlight is used to generate heat. The generated heat energy is used as an input to conventional power generation. The main goal of this method is to regulate the temperature of the oil in the output side of the loop at the required value, despite variations in the irradiation level, mirror reflectivity, or temperature of oil in the input side. The temperature was measured by using a thermocouple located in the receiver. This is a mechanical type of maximum power point tracking method. The main drawback of this method is that it did not consider the technical details of the PV system such as the dynamics of the converter and the PV array.

In [20] adaptive control of distributed collector solar fields was proposed. Distributed collector solar fields are used to collect and store energy from irradiance emitted from the sun. The mirrors are used to reflect irradiance from the sun to oil in a pipe. The main goal of this method is controlling outlet oil temperature to track the desired value by influencing oil inflow. This method solves the problem associated with the solar power generating system by using the mirrors to collect and produce more heat to the oil. This method is also a mechanical type of maximum power point tracking method. The drawback of this method is that the plant dynamics is not considered.

In [21] an adaptive control structure for MPPT of a single-phase grid-connected photovoltaic system was proposed. In the proposed method on-line sliding mode estimator was used to estimate three parameters that are dependent on environmental conditions such as irradiation and temperature, which are not simple to measure and vary in a non-uniform way. It reduces the requirement of sensors to measure these environmental variables. The drawback of this method is an oscillation of PV array output power due to the chattering problem of the sliding mode estimator.

In [22, 23] the tacking efficiency of most commonly used maximum power point tracking algorithms was presented by comparing them based on their performance, speed, and cost. The compared methods were OCV method, SCC method, incremental conductance method, and perturb and observe methods. From these algorithms, Incremental Conductance and perturb and observe are in general the most efficient of the investigated MPPT algorithms. Even though they show good performance compared with other MPPT algorithms they show an oscillation at MPP. This is their main drawback. Another drawback seen in P&O was it requires an external perturbation signal to drive power to its maximum power point. They also lack the tracking efficiency when the environment changes rapidly.

In [24] an optimized Adaptive P&O MPPT control for Photovoltaic Generation was proposed. Since the effectiveness of P&O depends on perturbation size they developed an adaptive P&O method that generates large perturbation size when the gap between current operating point and MPP was large and small perturbation signal when the gap between them was small. This method shows small oscillations exclusive of knowing the technical facts of the PV system, like traditional P&O method it uses an external signal due to this it needs additional circuits for perturbation purpose.

In [25] MPPT method for single-phase, a single-stage grid-connected PV system was proposed. They used RCC as the MPPT controller. This proposed method uses ripples generated in the array voltage when the voltage is subjected to grid frequency produced during power oscillation. As compared to other MPPT algorithms, RCC has the advantage of using inherent ripples which are produced in PV based power generation system to generate optimal duty ratio corresponds to MPP. However, its drawback it also exhibits an oscillation around MPP.

In [26] Model Reference Adaptive Control for MPPT in the PV system was proposed. In this proposed method the MRAC was used to reduce the transient oscillations caused when the duty cycle was updated, which is a problem not solved when other MPPT algorithms are used alone.

The proposed method shows an improvement in oscillation. However, the controller structure was a little bit complex, and also includes filters with arbitrarily selected constants. They can be randomly selected, so miss selection leads to a decrease in controller efficiency. In this proposed method the filters are also added when signals from the controller output and plant output were given back to the adaptation mechanism. This increases the bulkiness and the cost of the controller. Another demerit of this method is, in a Lyapunov design approach, the transfer function of state error-equation must be strictly positive real (SPR). Nevertheless, the transfer function of the realization is not SPR, this leads to another mathematical realization and increases the number of arbitrarily selected parameters.

As conferred in the presented review, each MPPT has its own merits and demerits. All try to find the best performance at the expense of cost/complexity or medium performance with adequate cost and comparative simplicity. The most common problem, most of the MPPT algorithms were facing is that an oscillation around MPP. Due to this reason, there is a power loss in the PV system. In this thesis, MRAC is used to overcome the above drawbacks. Since the critically damped reference model was used the proposed controller was efficient to reduce the oscillation that occurs around the MPP.

CHAPTER THREE
SYSTEM MODELING

3.1 Overview

This chapter covers the mathematical model for the PV system. Mathematical modeling of the photo-voltaic panel and dynamic model of DC-DC boost converter for the thesis is done on this chapter. The following sections present each of these in detail.

3.2 System model

As shown in figure 3.1 below, energy flows from the PV panel to the load. The solar radiation, which is not uniform, falls on the solar panel. The characteristic of the P-V curves varies frequently due to the variation in environmental conditions. The MPPT technique is employed when the current and voltage measurements obtained from the PV module. The output from RCC is the duty ratio (D) and it is given to the MRAC. The control signal from the MRAC was given to the DC-DC boost converter, which converts an unstable input voltage into an increased level stable output voltage. The MRAC is a class of adaptive control that, the required performance specifications are given in the reference model then the controlled plant responds like a reference model. The general system block diagram is shown in figure 3.1.

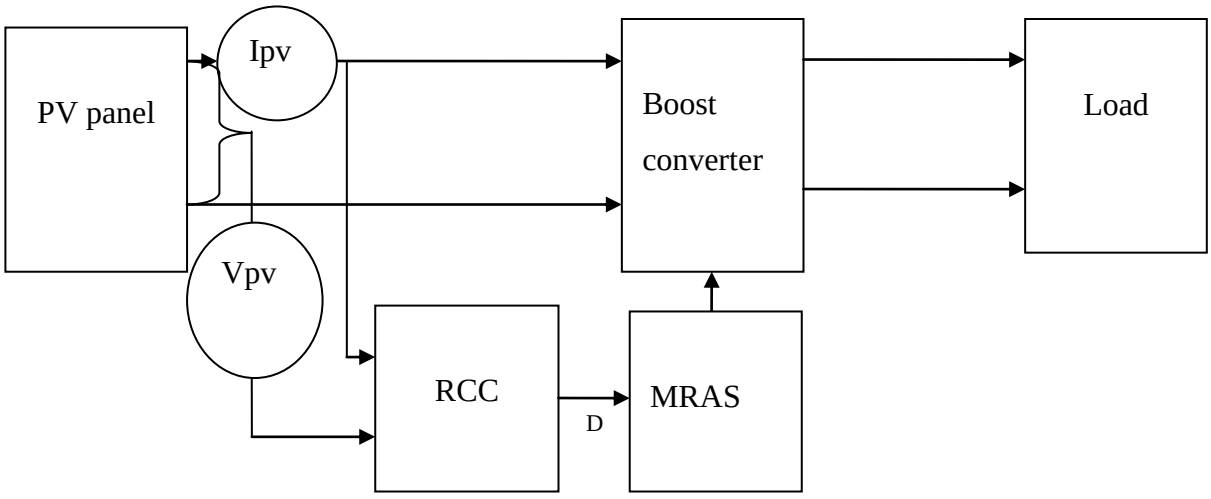

Figure 3.1: The general block diagram of solar energy control system.

3.3 Photovoltaic (PV) module design

PV array is a basic power converting element of a PV power generation system. The PV module output depends on three factors such as solar irradiation, temperature, and the PV array output voltage. Currently, PV cells are made from a p-n junction and they have a thin semiconductor layer. The electric current was produced from these cells when they are exposed to solar irradiation. The model consists of the series and the parallel resistances. The current generated by the photovoltaic cell is directly proportional to the amount of solar radiation reaches the cell surface. The single diode PV model is shown in figure 3.2 below.

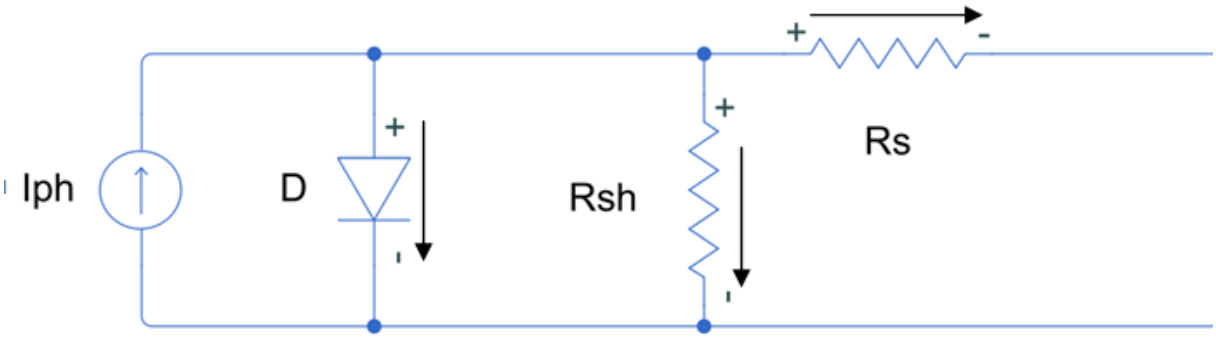

Figure 3.2: Single-diode model of the PV system.

Photocurrent for the PV panel will be

$$I_{ph} = (Isc + Ki(T - 298))\frac{G}{1000} \tag{3.1}$$

Saturation current

$$I_o = Irs\left(\frac{T}{Tn}\right)^3 .\exp\left[\frac{q.E_{go}\left(\frac{1}{Tn}-\frac{1}{T}\right)}{n.k}\right] \tag{3.2}$$

Reverse saturation current

$$I_{rs} = \frac{Isc}{\exp\left(\frac{q.V_{oc}}{n.N_S.K.T}\right)-1} \tag{3.3}$$

Current through shunt resistor

$$I_{sh} = \left(\frac{V+I.R_s}{R_{sh}}\right) \tag{3.4}$$

Output current

$$I_{pv} = I_{ph} - I_O\left[\exp\left(\frac{q.(V+I_{pv}.R_s)}{n.K.T.N_s}\right) - 1\right] - I_{sh} \tag{3.5}$$

Where

V is output voltage of a PV module (V)

I_{pv} is output current of a PV module (A)

T_n is the reference temperature = 298 K

v_{OC} is open circuit voltage (v)

G is the solar irradiation (w/m^2)

T is the module operating temperature in Kelvin

I_{ph} (photo current) is the light generated current in a PV module (A)

I_o is the PV module saturation current (A)

n is an ideality factor = 1.3

k is Boltzmann constant = 1.3805×10^{-23}J/K

q is Electron charge = 1.6×10^{-19} C

R_s is the series resistance of a PV module

I_{sc} is the PV module short-circuits current (A)

K_i is the short-circuit current temperature co-efficient at25^oC and$1000w/m^2$ = 0.0032

E_{go} is the band gap energy for semiconductor = 1.1 eV

N_s is the number of cells connected in series.

Rs is the series resistance

R_{SH} is shunt resistance

Ish is current in shunt resistance

3.4 DC-DC Boost Converter Model

A DC-DC boost converter is one of the types of power converters that transform input voltage to increased output voltage. It is one of the category switching mode power supply (SMPS) having a diode and a transistor for switching purposes and an inductor as a storage element. To reduce output voltage ripples, the capacitor as a filter is added to the output side of the converter. A DC-DC boost converter also said a step-up converter because it steps up an input voltage. In boost converter, the current in output side is smaller than the current input side so that, power is conserved. The buck converter and boost converter have the same components, but buck converter makes an output voltage less than its input voltage. In boost converter, the current starts to flow through the conductor when the switch is closed. This time is the beginning of the voltage conversion process. To study the characteristics of boost the following assumptions are made:

- DC-DC boost converter is working at steady state.
- The inductor current is continuous
- T is switching period, the switch is ON for time DT and it is OFF for time (1-D)T
- All elements of the converter are ideal

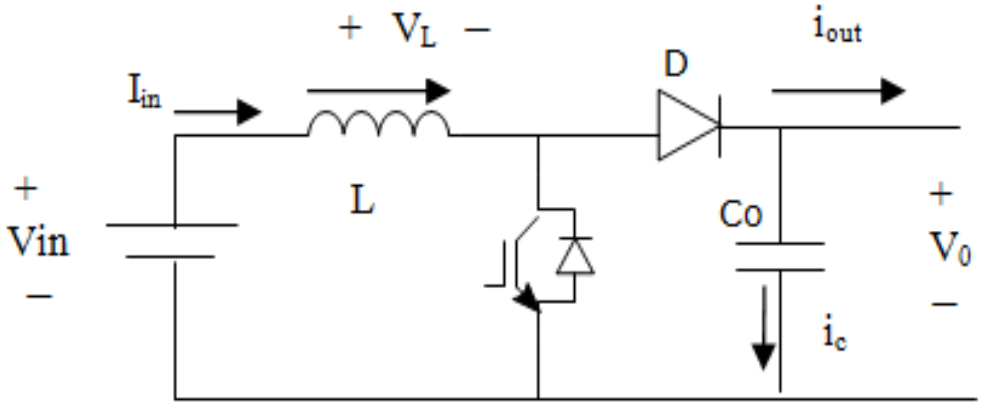

Figure 3.3: Boost converter schematic diagram

The basic idea that drives the boost converter is the propensity of an inductor to oppose variation in current. The inductor acts as both a load and a source. While it is charging it acts as a load, and it is discharging it acts as a source. The voltage produced at the discharging period is associated with the rate of change of current, therefore this gives different input and output voltage values.

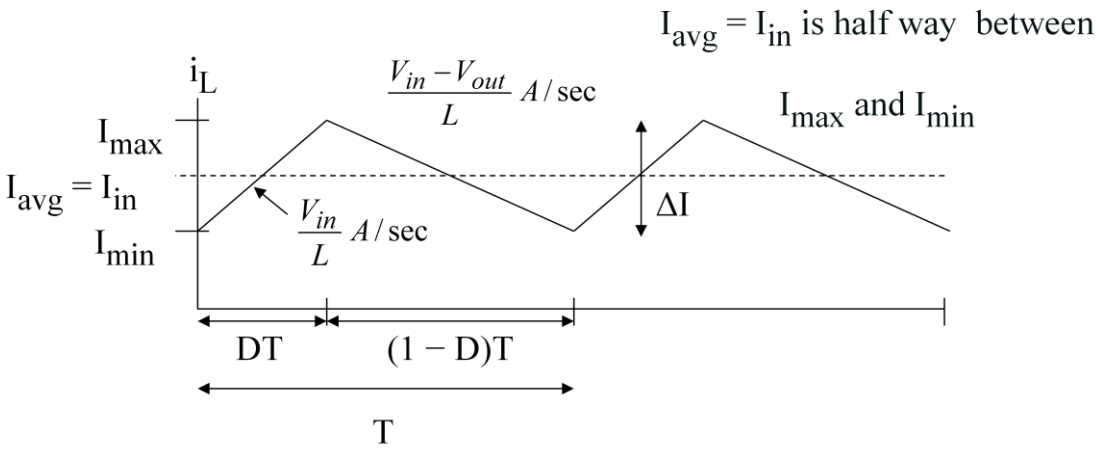

Figure 3.4: Waveforms of current in a boost converter operating in continuous mode.

The figure 3.5 shows switch is closed for DT seconds

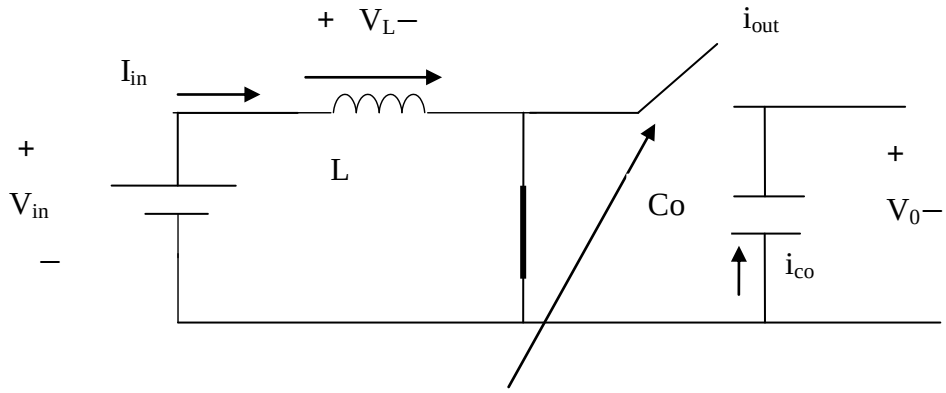

Reverse biased, thus diode is open.

Figure 3.5: Boost converter schematic diagram when the switch is ON for DT seconds.

When the switch S is closed, an On-state, this makes the current flow through the inductor. So, the input source (V_{in}) appear through an inductor, which causes a change in current (I_L) flowing through the inductor during a period (DT) by the formula::

$$\frac{di_L}{dt} = \frac{V_{in}}{L} \tag{3.6}$$

Moreover, at the end of the ON-state, the increase of I_L is, therefore:

$$\frac{di_L}{dt} = \frac{1}{L}\int_0^{DT} V_{in}\, dt = \frac{DT}{L} V_{in} \tag{3.7}$$

Where D is the duty cycle. It represents the fraction of the commutation period T during which the switch is closed. Therefore D ranges between 0 (S is OFF) and 1 (S is ON).

Figure 3.6 shows switch open for (1−D) T seconds

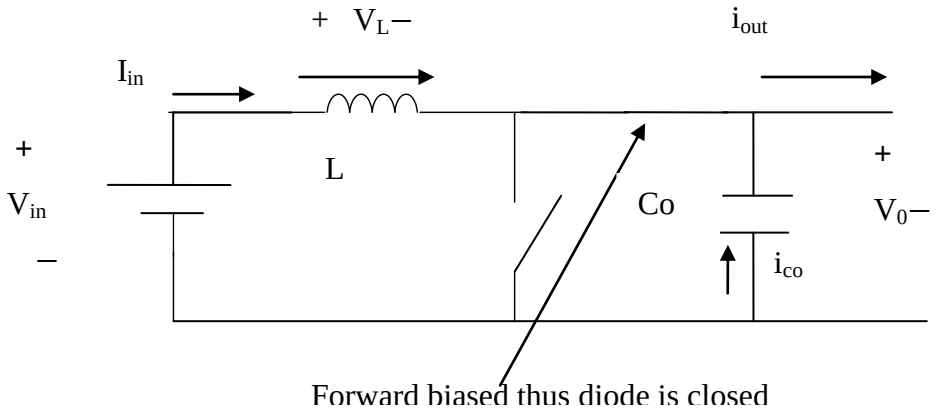

Figure 3.6: Boost converter schematic diagram when the switch is OFF for (1- D) T seconds.

During the Off-state, the switch S is open that the inductor current flows through the load. If we consider zero voltage drops in the diode, and a capacitor, that is large enough to store necessarily to provide constant voltage, then the inductor current I_L will be:

$$V_{in} - V_o = L\frac{dI_L}{dt} \tag{3.8}$$

Therefore, the variation of I_L during the Off-period is:

$$\frac{di_L}{dt} = \frac{1}{L}\int_0^{(1-D)T}(V_{in} - V_o)dt = (V_{in} - V_o)\frac{(1-D)T}{L} \tag{3.9}$$

Since the circuit is operating in a steady-state; all the elements of the converter are operating in a steady-state. Therefore, the amount of energy accumulated in each element of the converter at the start and the end of the commutation period is the same. Therefore, the inductor has the same stored energy at the beginning and the ending of the commutation period. This means the summation of the current at both states is zero:

$$\frac{dI_L}{dt}\text{ON state} + \frac{dI_L}{dt}\text{ OFF state} = 0 \tag{3.10}$$

By substituting equations from equation (3.7) and (3.9) in to (3.10) it will be

$$\frac{DT}{L}V_{in} + (V_{in} - V_o)\frac{(1-D)T}{L} = 0 \tag{3.11}$$

$$\frac{DT}{L}V_{in} + \frac{T}{L}V_{in} - \frac{DT}{L}V_{in} - \frac{T}{L}V_o + \frac{DT}{L}V_o = 0 \tag{3.12}$$

$$\frac{T}{L}V_{in} = \frac{T}{L}V_o - \frac{DT}{L}V_o \tag{3.13}$$

$$V_{in} = V_o - DV_o \tag{3.14}$$

$$V_{in} = (1-D)V_o \tag{3.15}$$

$$V_o = \frac{V_{in}}{(1-D)} \tag{3.16}$$

The equation (3.16) shows if there is a decrement in duty ratio (D), then there will be an increment in the output voltage (V_o), and vice versa.

Impedance matching:

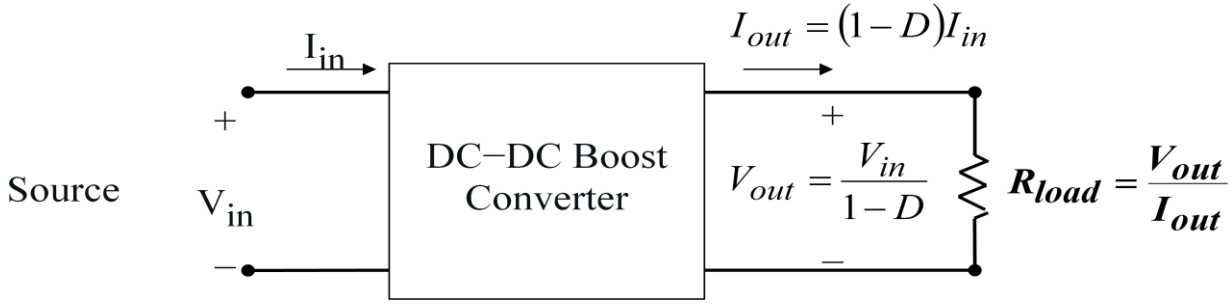

(a)

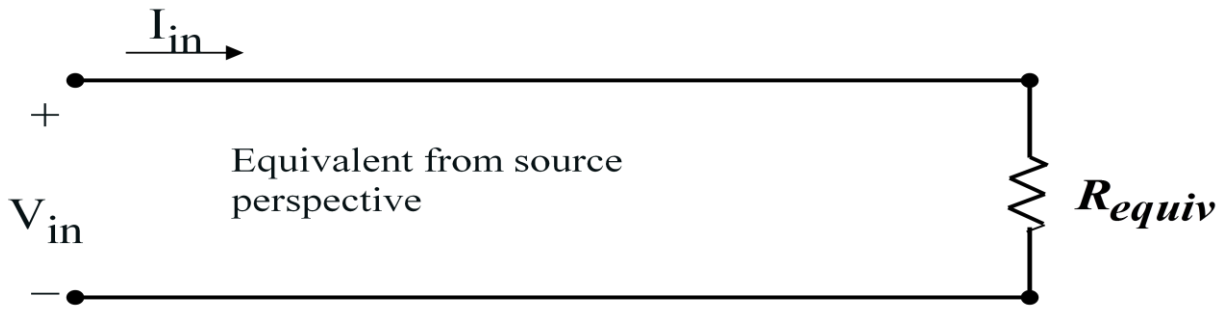

(b)

Figure 3.7: a) Impedance matching of boost converter b) Equivalent circuit from a source perspective

$$R_{equiv} = \frac{V_{in}}{I_{in}} = \frac{(1-D)V_{out}}{\frac{I_{out}}{1-D}} = (1-D)^2 \frac{V_{out}}{I_{out}} \tag{3.17}$$

In the solar power system, as shown in figure 3.1, the maximum power point tracking controller measures the solar module output voltage and current and generates the duty ratio to the switch S. This duty ratio is related to the photovoltaic output voltage as shown in equation (3.17).

$$V_{pv}=I_{pv}R_{equiv} \quad (3.18)$$

Substituting equation (3.17) in to (3.18)

$$V_{pv}=I_{pv}\,(1\text{-}D)^2R_{load} \quad (3.19)$$

Our main target is to develop a maximum power point controller that always computes the optimal duty ratio, which is useful to attain the MPP.

3.4.1 Dynamic modeling of a DC to DC boost converter

To study the dynamics of any converter, some transformations are necessary because the system is not linear, hence it is not possible to apply directly the Laplace Transform, and an averaging process is required. The converter which is going to be analyzed in this thesis is the one revealed in figure 3.8.

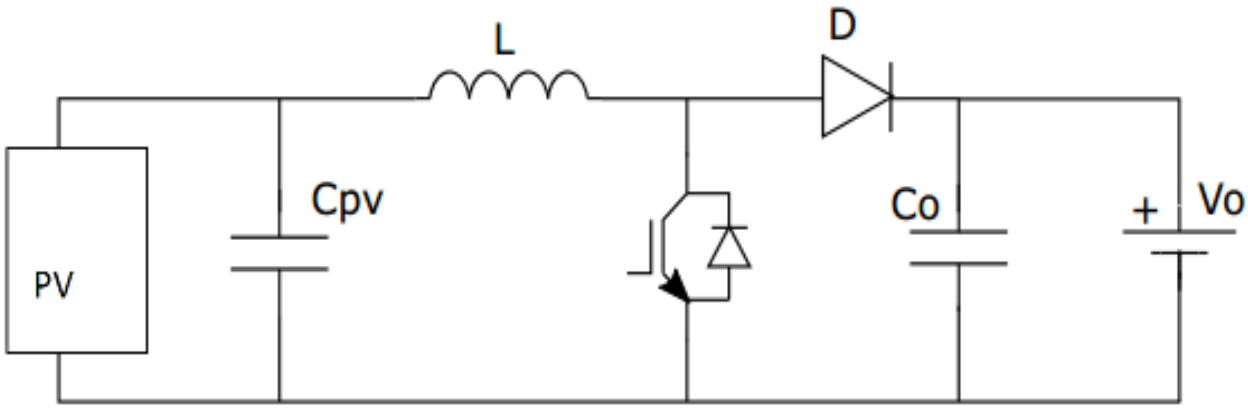

Figure 3.8: PV connected DC to DC converter

3.4.1.1 Large-signal Dynamic model

First of all the Large-signal AC model has been obtained analyzing the different interval conduction modes, on each interval, two parameters must be obtained to model the system, the current across the input capacitor ($I_c(t)$), and the voltage across the inductor ($V_L(t)$). The output capacitor is placed in shunt with an ideal voltage, and then this capacitor will be charged in every period. Before the analysis starts, it is necessary to apply the Norton theorem to the PV panel as shown in figure 3.9.

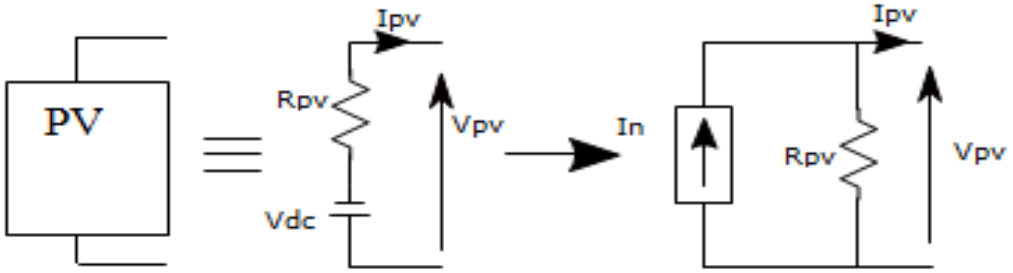

Figure 3.9: Norton transformation

Case 1: when Switch (ON)

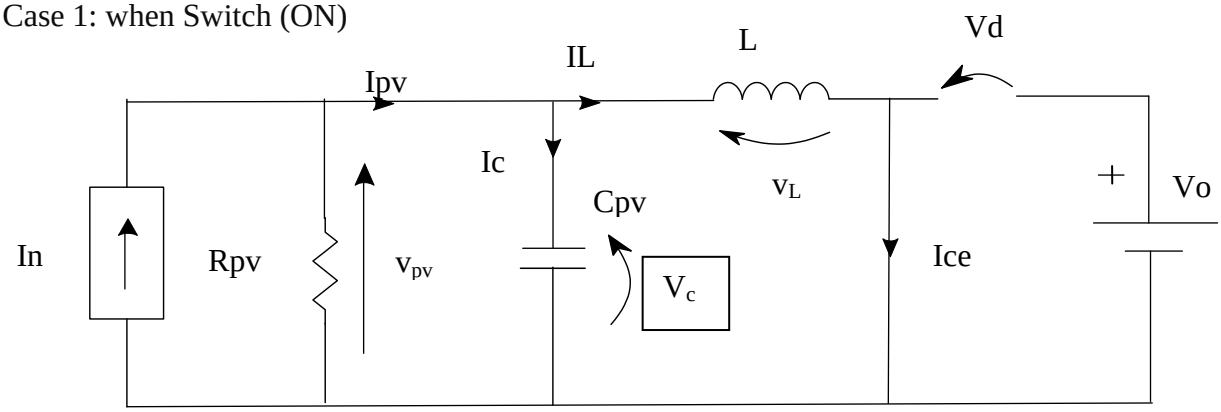

Figure 3.10: The circuit diagram for T_on period

In this mode, the switch is closed for the duration DT seconds and the diode is reverse biased, and the current through the inductor increases. Based on figure 3.10 an inductor voltage and the capacitor current will be described as follows:

$$V_L(t) = L\frac{d\, I_L(t)}{dt} = V_c(t) \tag{3.20}$$

$$I_c(t) = C\frac{dV_c(t)}{dt} = I_n(t) - I_L(t) - I_{RPV}(t) \tag{3.21}$$

Case 2: when switch is off

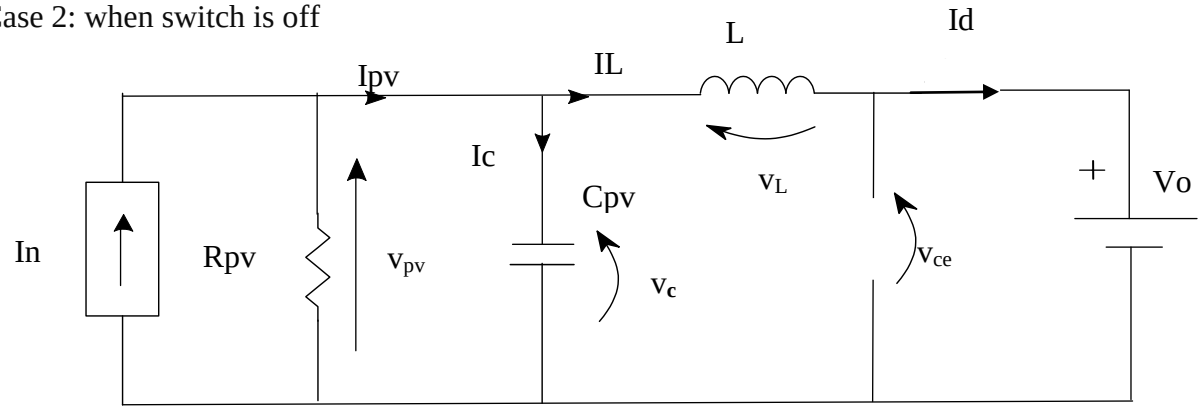

Figure 3.11: The circuit diagram when the switch is off(T_off period)

In this mode, the switch is off for the duration $(1 - D)T$ and the diode is forward biased. Current through the inductor continues to flow through the diode. From the above diagram, the voltage across the inductor and the current through the capacitor will be described as follows.

$$V_L(t) = L\frac{diL(t)}{dt} = V_c(t) - V_o(t) \tag{3.22}$$

$$I_c(t) = C\frac{dV_c(t)}{dt} = I_n(t) - I_L(t) - I_{Rpv}(t) \tag{3.23}$$

The diode is conducting current, which is equal to the inductor current, then:

$$I_D(t) = (1\text{-}d(t)).I_L(t) \tag{3.24}$$

The averaged state space model can be found by calculating the essential derivatives and output equations independently when the switch closed and open; and finally by multiplying those equations by the duty cycle (d (t)) and its complement $(1 - d(t))$ and adding them together [27]. Then the average model can be obtained:

$$L\frac{diL(t)}{dt} = d(t)Vc(t) + \big(1 - d(t)\big)(Vc(t) - Vo(t)) \tag{3.25}$$

$$C\frac{dVc(t)}{dt} = d(t)\big(I_n(t) - I_L(t) - I_{Rpv}(t)\big) + \big(1 - d(t)\big).\big(I_n(t) - I_L(t) - I_{Rpv}(t)\big) \tag{3.26}$$

The large-signal dynamic model has been defined in equations (3.25) and (3.26).To apply the Laplace transform, to get the transfer function of the system, the above equations are not linear because they depend on the time, then they should be linearized. To obtain the linearized equations Small-signal modeling is used which is a common analysis technique in electronics engineering to approximate the behavior of electronic circuits.

3.4.1.2 Small-Signal Dynamic model

To obtain the small-signal model which is the linearized form of the system substituting every variable by its steady-state variable and small-signal variation (AC perturbation) about the steady-state at the equilibrium point, which is represented by a hat, in the large average signal model we will get.

$$x(t) = \hat{x}(t) + X \tag{3.27}$$

Where X is steady-state variable and $\hat{x}(t)$ is small-signal variation. By applying equation (3.27) in the equations (3.25) and (3.26) of a large-signal model the system will be linearized as follows.

i) The diode can be linearized as:

Equation (3.24) can be rewritten as

$$\hat{\imath}_D(t) + I_D = \left(1 - \hat{d}(t) - D\right)(\hat{\imath}_L(t) + I_L) \tag{3.28}$$

$$\hat{\imath}_D(t) + I_D = \hat{\imath}_L(t) + I_L - \hat{d}(t)\hat{\imath}_L(t) - \hat{d}(t)I_L - D\hat{\imath}_L(t) - DI_L) \tag{3.29}$$

By removing steady state and neglecting product of small signals

$$\hat{\imath}_D(t) + I_D = (1 - D)I_L - \hat{d}(t)I_L + (1 - D)\hat{\imath}_L(t) \tag{3.30}$$

$$\hat{\imath}_D(t) = (1 - D)\hat{\imath}_L(t) - \hat{d}(t)I_L) \tag{3.31}$$

ii) The capacitor can be linearized as:

Equation 3.26 can be rewritten as:

$$C\frac{d(\hat{v}c+Vc)}{dt} = \left(\hat{d}(t) + D\right)\left(\hat{\imath}_n(t) + I_n - \hat{\imath}_L(t) - I_L - \hat{\imath}_{Rpv}(t) - I_{Rpv}\right) + \left(1 - \hat{d}(t) - D\right)(\hat{\imath}_n(t) + I_n - \hat{\imath}_L(t) - I_L - \hat{\imath}_{Rpv}(t) - I_{Rpv}) \tag{3.32}$$

By rearranging equation (3.32)

$$C\frac{d(\hat{v}c)}{dt} = \hat{\imath}_n(t) + I_n - \hat{\imath}_L(t) - I_L - \hat{\imath}_{Rpv}(t) - I_{Rpv} \tag{3.33}$$

iii) The inductor can be linearized as:

Equation (3.25) can be rewritten as:

$$L\frac{d(\hat{\imath}L+IL)}{dt} = \left(\hat{d}(t) + D\right)(\hat{v}_c(t) + V_c) + (1 - \hat{d}(t) - D)(\hat{v}_c(t) + V_c - \hat{v}_o(t) - V_o) \tag{3.34}$$

By rearranging equation (3.34)

$$L\frac{d(\hat{\imath}L)}{dt} = \hat{v}_c(t) + V_c - (1 - D)\hat{v}_o(t) + \hat{d}(t)V_o \tag{3.35}$$

For the linearized equation the circuit can be drawn as shown in figure 3.12.

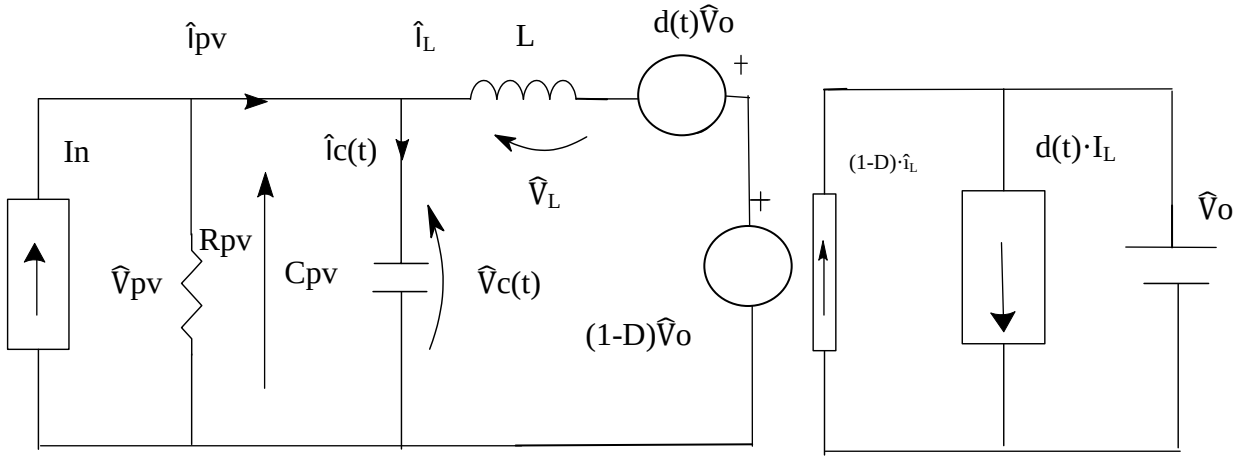

Figure 3.12: Small-signal model type one

The above figure which is shown in figure 3.12 can be reduced another circuit which is shown in figure 3.13 below

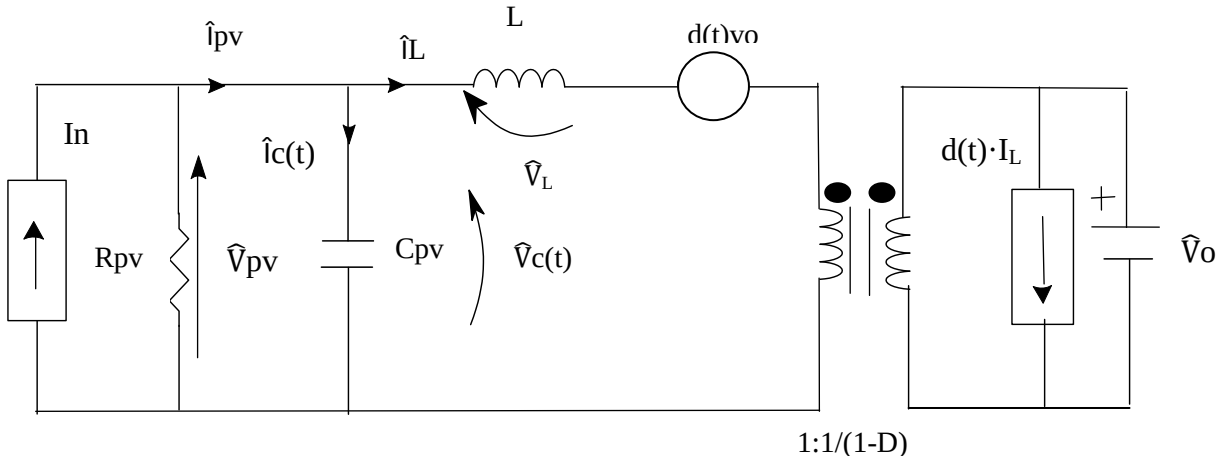

Figure 3.13: Small-signal model type two

The small-signal model in figure 3.13 can also be rearranged as

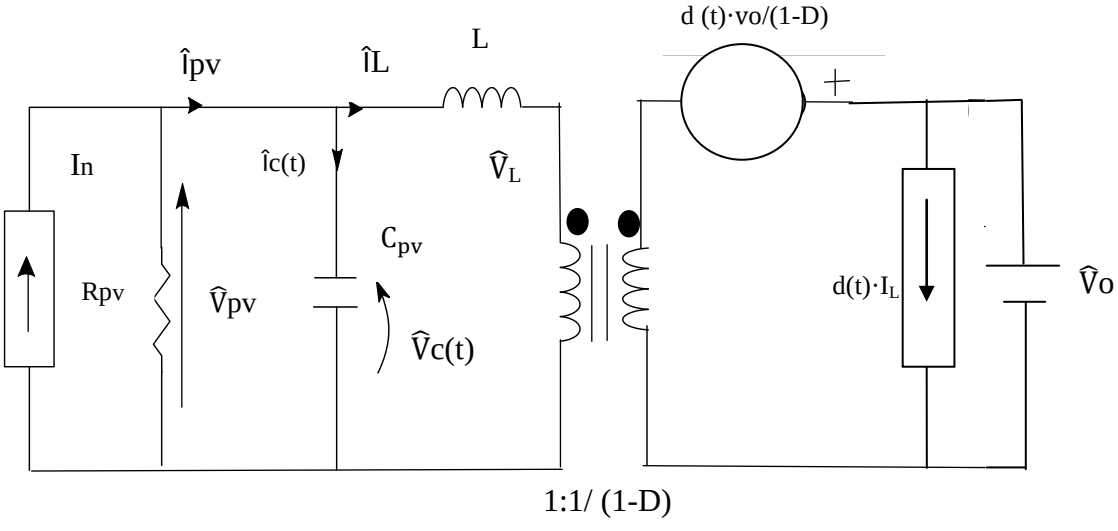

Figure 3.14: Small-signal model type three

From the above three models, the final canonical form of the system will be

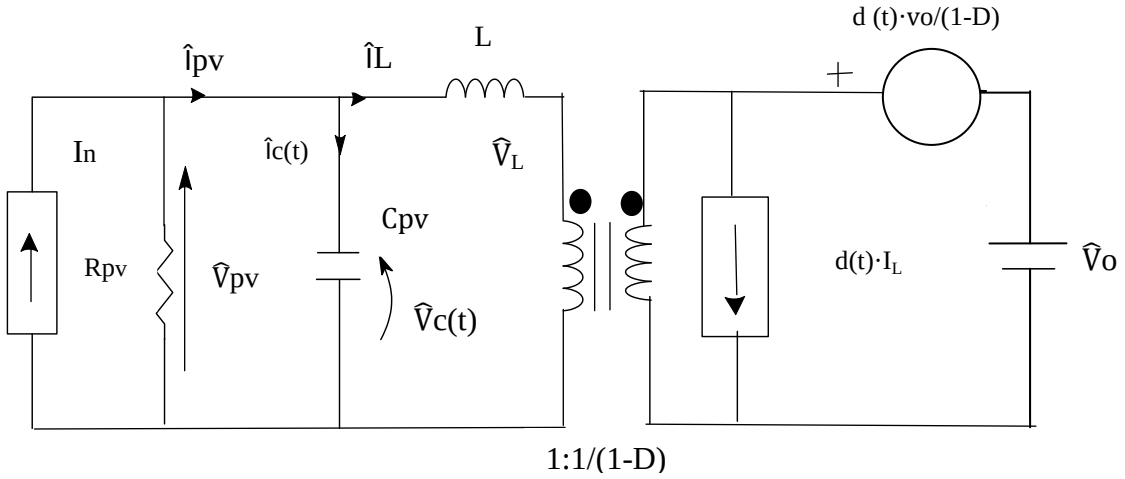

Figure 3.15: Canonical form of small-signal model.

Finally to obtain the transfer function which relates $\hat{v}_{PV}$ and $\hat{d}$ some considerations should be taken [28]. These considerations are:

$$\begin{cases} \hat{v}_o = 0 \\ i_n = 0 \end{cases} \tag{3.36}$$

Starting from considerations on equation (3.37) the circuit shown in figure 3.15 can be reduced to figure 3.16 shown below.

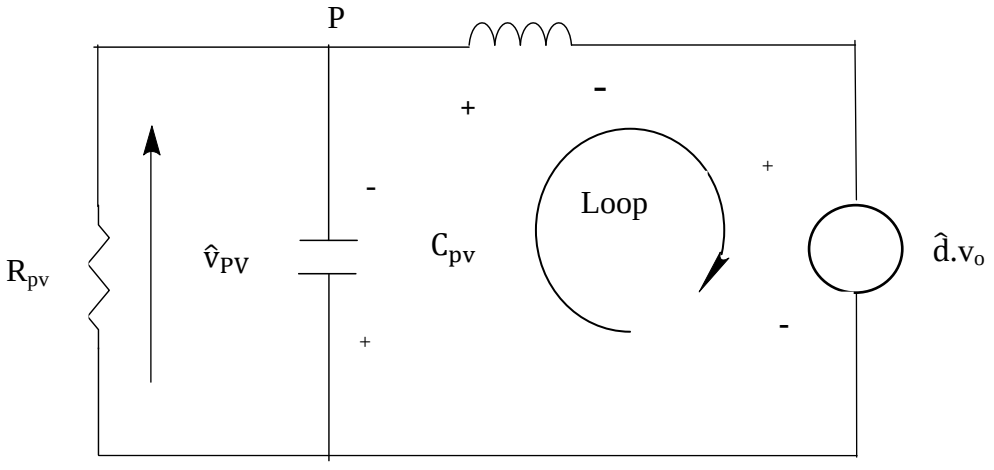

Figure 3.16: Small-signal circuit of the PV conversion system.

By applying KCL at a point P and KVL at loop1 of the circuit shown above in figure 3.16

KCL at point p will be

$$\hat{\imath}_L = \hat{\imath}_{PV} + \hat{\imath}_c \tag{3.37}$$

KVL at loop1 will be

$$\hat{v}_L + \hat{v}_{pv} + \hat{d}.V_o = 0 \tag{3.38}$$

$$L\frac{d\hat{i}_L}{dt} + \hat{v}_{pv} + \hat{d}.V_o = 0 \tag{3.39}$$

By substituting equation (3.37) in to (3.39)

$$L\frac{d(\hat{i}_L+\hat{i}_c)}{dt} + \hat{v}_{pv} + \hat{d}.V_o = 0 \tag{3.40}$$

$$L\frac{d}{dt}\left(\frac{\hat{v}_{pv}}{R_{pv}} + C_{pv}\frac{d\hat{v}_{pv}}{dt}\right) + \hat{d}.V_o = 0 \tag{3.41}$$

Applying Laplace transform on equation (3.41) then,

$$\hat{v}_{pv} + LS\frac{\hat{v}_{pv}}{R_{pv}} + LC_{pv}S^2\hat{v}_{pv} = -\hat{d}.V_o \tag{3.42}$$

$$\hat{v}_{pv}\left(LC_{pv}S^2 + \frac{LS}{R_{pv}} + 1\right) = -\hat{d}.V_o \tag{3.43}$$

$$\frac{\hat{v}_{pv}}{\hat{d}} = -\frac{\frac{V_o}{LC}}{s^2+\frac{1}{C_{pv}R_{pv}}S+\frac{1}{LC}} \tag{3.44}$$

Equation (3.44) is second order equation. The negative sign shows the reverse relationship between the change of a solar module voltage (V_{pv}) and change of duty cycle (d).

3.4.2 Parameter selection for DC-DC boost converter

The specifications of the boost converter are:

Table 3.1: Specifications of the DC-DC boost converter for the given model

Minimum input voltage ($V_{in\text{-}min}$)	25v
Switching frequency (f_s)	20000Hz
Minimum output voltage ($V_{out\text{-}min}$)	48v
Output power (P_{out_min})	240 watt
Efficiency (η)	0.9
dv _ percent	1%

From specifications given in table 3.1 we can calculate the parameters of boost converter as follows:

Output voltage ripples (dv):

$$dv = V_{out\text{-}min} \text{ x } dv \_ \text{percent} \tag{3.46}$$

$$dv = 48 \text{ x } 1/100 = 0.48v$$

Duty cycle (D):

$$D = 1 - \left(\frac{Vin-min}{Vout-min} \text{x } \eta\right) \tag{3.47}$$

$$D = 1-\left(\frac{25x0.9}{48}\right) = 0.53125$$

Output current (I_{out_min}):

$$I_{out\_min} = \frac{P_{out\_min}}{V_{out\_min}} \tag{3.48}$$

$$I_{out\_min} = \frac{240 \text{ watt}}{48 \text{ v}} = 5A$$

Input current ripple (di)

$I_{ripple:}$A good estimation for the inductor ripple current is 20% to 40% of the output current.

$$di = I_{ripple} \text{ x } I_{out\_min} \left(\frac{V_{out\_min}}{V_{in\_min}}\right) \tag{3.49}$$

$$di = 0.4x5(48/25) = 3.48A$$

Inductance (L):

An inductor magnetic field is used switching converters to alternately store energy and release it to the load at a different voltage. The higher the inductor value, the higher will be the maximum output current because of the reduced ripple current Therefore the inductor must always have a higher current rating than the maximum allowable current because of the current increases with decreasing inductance.

$$L = \frac{V_{in-min}(v_{out\_min} - v_{in\_min})}{di \text{ x } f_s \text{ x } v_{out\_min}} \tag{3.50}$$

$$L=\frac{25 \text{ x } (48-25)}{3.48 \text{ x } 20000 \text{ x } 48} = 1.559\text{x}10^{-4} \text{ H}$$

Output Capacitance(C):

The value of output capacitor should be calculated to give the desired peak-to-peak output voltage ripple and is given by

$$C =\frac{I_{out\_min} \text{x } D}{f_s \text{ x } dv} \tag{3.51}$$

$$C=\frac{5A \text{ x } 0.53125}{20000 \text{ x } 0.48} = 2.767\text{x}10^{-4}\text{F}$$

Input capacitance (C_{pv}):

The input capacitor Cpv is the capacitor linked in parallel with the PV array. It is the capacitor at the input of the boost converter. The decoupling capacitor is calculated as:

$$C_{pv}=\frac{I_{out\_min} \text{x } D^2}{0.02(1-D)f_s V_{in\_min}} \tag{3.52}$$

$$C_{pv} =\frac{5\text{x}(0.53125)^2}{0.02(1-0.53125)20000\text{x}25} =1.015\text{x}10^{-4}\text{F}$$

Load(R):

$$R=\frac{V_{out\_min}}{I_{out\_min}} \tag{3.53}$$

$$R=\frac{48V}{5A} = 9.6\Omega$$

Table 3.2: The summary of parameter of DC-DC boost converter

Inductance (L):	$1.559\text{x}10^{-4}$ H
Output Capacitance(C):	$2.767\text{x}10^{-4}$F
Input capacitance(C_{pv}):	$1.015\text{x}10^{-4}$F
Load(R):	9.6Ω

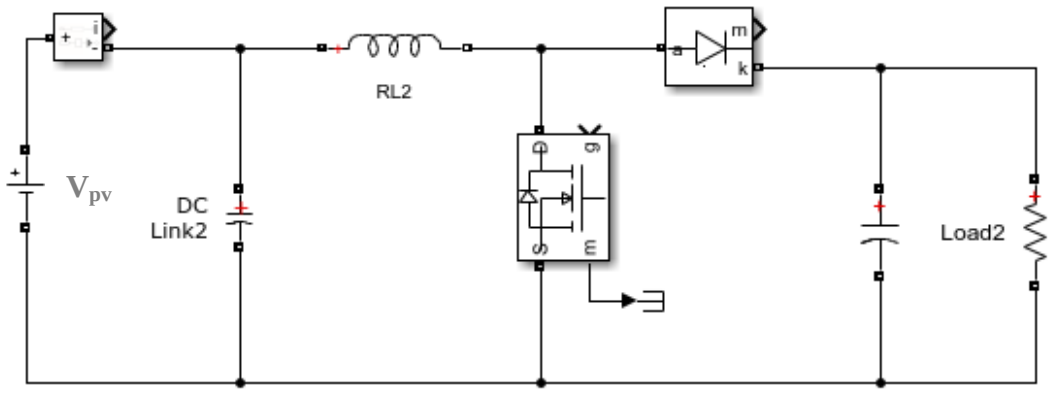

Figure 3.17: Simulation model of DC-DC boost converter using MATLAB/Simulink.

CHAPTER FOUR
CONTROLLER DESIGN

4.1 Ripple correlation control (RCC)

The ripple correlation control correlates the voltage and power of the photovoltaic panel to know the location of V_{pv} weather it is in the left side or right side of the V_{mpp}. When the PV panel is connected to boost converter, the array voltage consists of a dc constituent V_{pv} and a ripple constituent $\tilde{V}_{PV}$. For a certain temperature and solar irradiation, the PV output voltage is accustomed and the output power, P_{pv} changes. The photovoltaic output power also contains a dc constituent P and a ripple constituent $\tilde{p}$. PV output power shows nonlinear behavior as shown in Figure 2.1. The temperature and solar irradiation the affect moving direction power curve. So, the direction of MPP on the curve moves as well. The objective of this section is to force V_{pv} to track V_{mpp} as fast as likely, despite variation in environmental conditions. The PV module output power is a function of solar irradiation and temperature. Thus, changes in these irradiances and temperature will bring different power values. The MPPT controller senses the voltage and current from the solar module and produces a duty ratio to the switch of boost convertor. In this thesis, Ripple Correlation Control (RCC) is primarily designed to find a duty ratio which corresponds to the maximum power point in various temperature and solar irradiance level. The ripple correlation control operates like P&O, but the only difference is ripple correlation control inherent ripple components of current and voltage available in a boost converter are used to determine the location of current operating point and MPP. The operation of RCC is stated as follows. When the product of the time-based derivatives of the PV panel output voltage (V_{pv}) and power (p_{pv}) is positive the current operating point is to the left side of the maximum power point, the product of the time-based derivatives of the PV panel output voltage (V_{pv}) and power (p_{pv}) is negative the current operating point is to the right side of the maximum power point, and equal to zero at the maximum power point. Mathematically it can be expressed as:

$$\frac{dp_{pv}}{dt}\frac{dV_{pv}}{dt} > 0 \quad \text{When } V_{pv} < V_{mpp} \tag{4.1}$$

$$\frac{dp_{pv}}{dt}\frac{dV_{pv}}{dt} < 0 \text{ When } V_{pv} > V_{mpp} \tag{4.2}$$

$$\frac{dp_{pv}}{dt}\frac{dV_{pv}}{dt} = 0 \quad \text{When } V_{pv} = V_{mpp} \tag{4.3}$$

The equations represented above leads to develop an RCC law

$$\frac{dd(t)}{dt} = k\frac{dp_{pv}}{dt}\frac{dV_{pv}}{dt} \tag{4.4}$$

To obtain the duty cycle, we can apply the integration on both sides of the equation (4.4)

$$d = k \int \frac{dp_{pv}}{dt} \frac{dV_{pv}}{dt} \tag{4.5}$$

Where d represents the duty ratio and k is a negative constant because V_{pv} and I_{pv} have an inverse relationship. The array voltage increases and decreases as the duty cycle decrease and increase respectively, so adjusting the duty cycle should provide the correct movement of V_{pv} to V_{mpp}. From the above relationship, if increasing array output voltage causes an increase of array output power shows the current operating point is to the left of the MPP. To move the operating point towards the maximum point the duty ratio should be decreased; which causes an increase of V_{PV} as stated in (3.20). If increasing array output voltage causes the decrease in array output power, then thus duty ratio should be increased to decrease array output voltage towards the maximum power point. In place of derivatives, the available ripples in PV voltage and current are used. The derivatives can be approximated by High pass filters or low pass filters. In this thesis, the derivatives are approximated with high-pass filters. The cutoff frequency of two high pass filters used in RCC should be the same, if not it results in a phase change in power and voltage or current.

Generally, the ripple content of a general time-varying quantity (t) can be expressed as:

$$\tilde{y}(t) = y(t) - \bar{y}(t) \tag{4.6}$$

Where $\tilde{y}(t)$ represents the ripple content, and $\bar{y}(t)$ represents the moving average component. The general quantity, $y(t)$ can represent PV array voltage, V_{pv} (t); current, i_{pv} (t); or power, P_{pv}(t).The power can be obtained by multiplying the voltage and the current as

$$P_{pv}(t) = V_{pv}(t)\, i_{pv}(t) \tag{4.7}$$

The implementation block of RCC is indicated in figure 4.1. Two high-pass filters are implemented in a place of derivative in the control law. To calculate array power and the product for the integrand of equation (4.1) two multipliers are used.

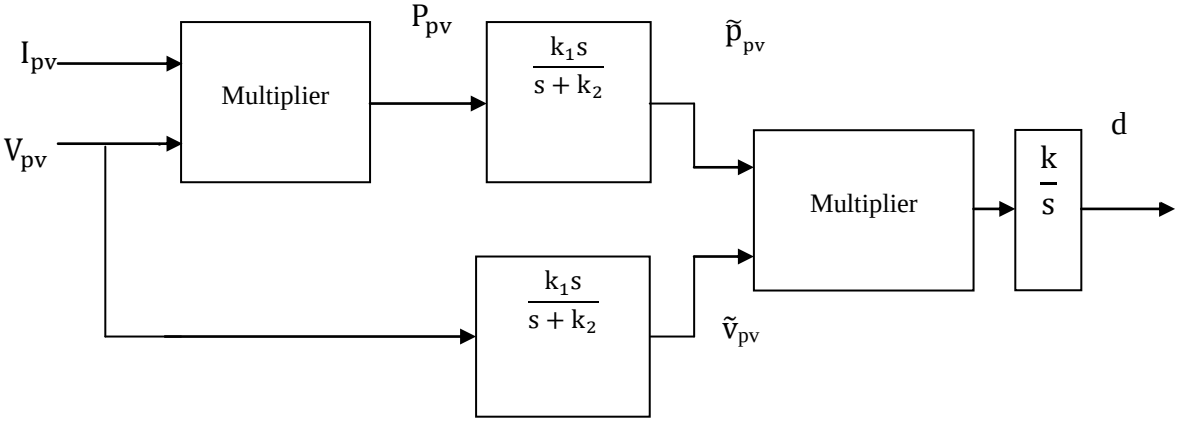

Figure 4.1: General block diagram of RCC.

Basically in ripple correlation, the time derivatives of power and current are calculated; which is non-zero due to the presence of inherent ripples present due to converter switching. The ripple component can be separated by using two high pass filters as shown in figure 4.1. Since the available ripples are inherent due to converter switching, the corner frequencies for the two filters must be less than the ripple frequency. In this thesis, the cutoff frequency used for the high pass filter is 1500Hz.

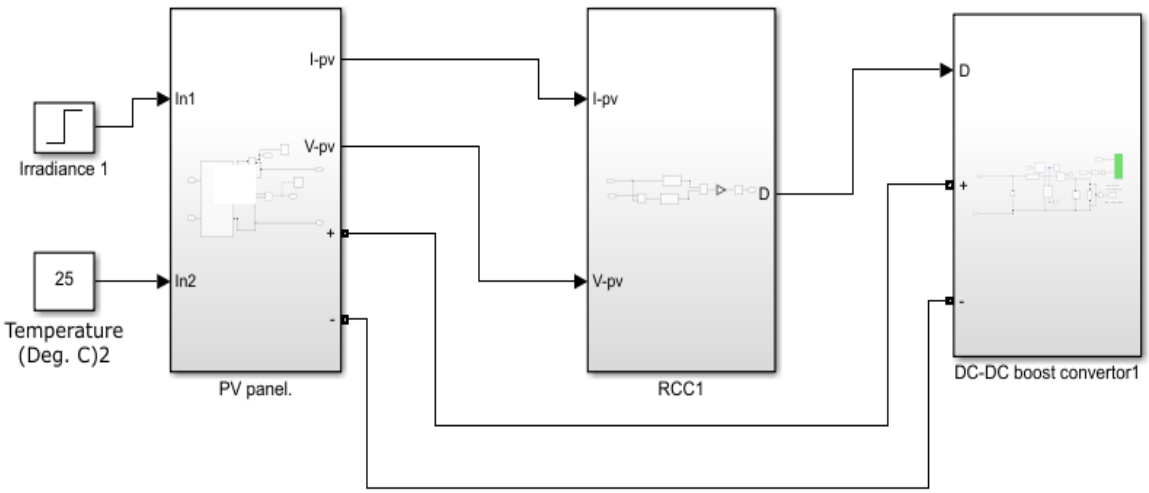

Figure 4.2: Simulink model of MPPT using Ripple correlation control.

4.2 MRAC controller

The basic idea behind Model Reference Adaptive Control (MRAC) is an adaptive control technique where the performance specifications are given in terms of a reference model so that the response of the controlled plant and the response of a reference model with desired dynamics

will be similar, even though there are changes in the plant parameters. The model was selected in a way that it gives the ideal response of the process is as desired. The adaptation mechanism can be used to adjust the controller parameters automatically. The parameter adjustment mechanism can be the MIT rule or Lyapunov stability method. A stable closed-loop system can be guaranteed by the Lyapunov rule but MIT can't. Therefore, the Lyapunov stability method is used in this thesis, which avoids the drawback present in the MIT rule. The error coming from the outputs of the controlled plant and the reference model acts as input to the adaptation mechanism.

In the RCC, the duty ratio is varying continuously during searching the maximum power point. This variation causes transient oscillation in the photovoltaic outputs. This makes the system to oscillate at a maximum power point. To reduce this oscillation, we should have to make the system have to be critically damped. To achieve this objective reference model with critically damped characteristics was used.

During adaptation, the error results from the output of the plant and the reference model is used to adjust the parameters in the controllers. Proper tuning of the controller parameters assists the output of the plant to follow the output of the reference model, which makes the error converge to zero and the maximum power point is obtained. The MRAC structure consists of four main parts: the plant, the controller, the reference model, and the adjustment mechanism (adaptation law).

Reference Model: Is a part of the controller that contains the required performance. In general, the adaptive controller enforces the actual plant to perform similarly with that of the reference model. In this thesis the reference model which is a system with a damping ratio of 1.

Controller: It consists of some regulating parameters. During the design, linearization is required to get the adaptation mechanism of the controller with assured stability and tracking convergence. An adaptation gain is the main factor to affect the controller parameters.

Adaptation Mechanism: It is a way to regulate the parameters in the control system. The adaptation mechanism seeks the parameters to make the response of the controlled plant similar to the reference model. It is planned to assure the stability of the system and minimize tracking error.

3.4.4.1 Lyapunov stability method (Lyapunov rule)

This method is one of the methods of designing the adaptive controller. It attempts to find the Lyapunov function and an adaptation mechanism. Also, this method ensures the stability of the control parameters of the system. In this thesis, the design using the Lyapunov stability method (Lyapunov rule) was used. When designing the MRAC using the Lyapunov rule, it can be chosen the reference model, the controller structure, and the tuning gains for the adjustment mechanism. While using RCC the PV outputs are oscillating due to variation in duty ratio. To reduce this the reference model with a damping ratio equal to 1 is used. The variable duty ratio is given to the MRAC, which is the output of RCC. The transfer function $G_p(s)$ represents the linearized form of the photovoltaic power generating system. The signal $u_c(s)$ is the input to the plant model and also the controller's output. $y_p(s)$ is the output of the plant model.

$$G_p(s) = \frac{y_p(s)}{u_c(s)} = \frac{k_p}{s^2 + a_p s + b_p} \tag{4.8}$$

The value of constants can be obtained for equation (4.8) can be linearized circuit of the boost converter. The specific values were shown in Table 3.2. The reference model was selected as:

$$G_m(s) = \frac{y_m(s)}{u(s)} = \frac{k_m}{s^2 + a_m s + b_m} \tag{4.9}$$

The parameters of the reference model should be more close to the plant model. Steps required deriving the adaptive law for the controller's parameter in MRAC.

- Determine the controller structure.
- Derive the error equation.
- Find a Lyapunov equation.
- Determine the adaptation law that satisfies the Lyapunov theorem.
- Finally, test and validate the result.

In this method, the reference model is usually assumed as shown below

$$\frac{dym}{dt} = -a_m y_m + b_m u_c \tag{4.10}$$

And the process which is going to be controlled as

$$\frac{dyp}{dt} = -a_p y_p + b_p u \tag{4.11}$$

The control law is chosen as:

$$u=\theta_1 u_c - \theta_2 y_p \tag{4.12}$$

Where;

y_p- is the plant output

y_m - is reference model output

θ_1 and θ_2- are the parameters of the controller to be updated

u - is the input from RCC

u- is the controller output signal

e - is the difference between actual plant output and reference model output

Then the error will be the difference between the actual plant output and the reference model output.

$$e = y_p - y_m \tag{4.13}$$

Our goal is to make the error small as much as possible, it is natural to derive a differential equation for the error. Then from equation (4.13) we can drive the differential equation for the error as follows.

$$\frac{de}{dt} = \frac{dy_p}{dt} - \frac{dy_m}{dt} \tag{4.14}$$

$$\frac{de}{dt} = -a_p y_p + b_p u - (-a_m y_m + b_m u_c)` \tag{4.15}$$

$$\frac{de}{dt} = -a_p y_p + b_p u + a_m y_m - b_m u_c \tag{4.16}$$

Substituting equation (4.12) to equation (4.16)

$$\frac{de}{dt} = -a_p y_p + b_p (\theta_1 u_c - \theta_2 y_p) + a_m y_m - b_m u_c \tag{4.17}$$

$$\frac{de}{dt} = -a_p y_p - b_p \theta_2 y_p + a_m y_m + (b_p \theta_1 - b_m) u_c \tag{4.18}$$

$$\frac{de}{dt} = -a_p y_p - a_m y_p + a_m y_p - b_p \theta_2 y_p + a_m y_m + (b_p \theta_1 - b_m)\, u_c \tag{4.19}$$

$$\frac{de}{dt} = a_m (y_m - y_p) - y_p (b_p \theta_2 - a_p + a_m) + (b_p \theta_1 - b_m)\, u_c \tag{4.20}$$

After some rearrangements

$$\frac{de}{dt} = -a_m e - y_p (b_p \theta_2 - a_m + a_p) + (b_p \theta_1 - b_m)\, u_c \tag{4.21}$$

The next step is constructing a parameter adjustment mechanism that will drive the parameters θ_1 and θ_2 to their desired values. For this purpose, assume that $b\gamma > 0$ and introduce the following quadratic function.

$$V(e, \theta_1, \theta_2) = \frac{1}{2}\left(e^2 + \frac{1}{b_p \gamma}(b_p \theta_2 + a_p - a_m)^2 + \frac{1}{b_p \gamma}(b_p \theta_1 - b_m)^2\right) \tag{4.22}$$

This function is zero when an error is zero and the controller parameters are equal to the correct values. For this function to qualify as Lyapunov function, the derivative $\frac{dv}{dt}$ must be negative definite.

The derivative is:

$$\frac{dv}{dt} = e\frac{de}{dt} + \frac{1}{\gamma}(b_p \theta_2 + a_p - a_m)\frac{d\theta_2}{dt} + \frac{1}{\gamma}(b_p \theta_1 - b_m)\frac{d\theta_1}{dt} \tag{4.23}$$

By substituting equation (4.1) to(4.23) and by rearranging

$$\frac{dv}{dt} = -a_m e^2 + \frac{1}{\gamma}(b_p \theta_2 + a_p - a_m)\left(\frac{d\theta_2}{dt} - \gamma y_p e\right) + \frac{1}{\gamma}(b_p \theta_1 - b_m)\left(\frac{d\theta_1}{dt} + \gamma u_c e\right) \tag{4.24}$$

Equation above, Lyapunov function, is negative if and only if

$$\frac{d\theta_2}{dt} - \gamma y_p e = 0 \quad \text{And} \quad \frac{d\theta_1}{dt} + \gamma u_c e = 0 \tag{4.25}$$

From equation (4.25) the parameters are updated as

$$\frac{d\theta_2}{dt} = \gamma y_p e \quad \text{And} \quad \frac{d\theta_1}{dt} = \gamma u_c e \tag{4.26}$$

Then finally the Lyapunov function will be

$$\frac{dv}{dt} = -a_m e^2 \tag{4.27}$$

The derivative of V with the respect to time t is negative semi definite. This implies that $V(t) \leq V(0)$ and thus that e, θ_1 and θ_2 must be bounded and $y_p = e + y_m$ also is bounded.

From equation (3.44)

$$G_p(s) = \frac{\frac{v_o}{LC_{pv}}}{s^2 + \frac{1}{C_{pv}R_{pv}}S + \frac{1}{LC_{pv}}} = \frac{k_p}{s^2 + a_p s + b_p} \tag{4.28}$$

The constants of equation (4.28) can be calculated by taking the parameter values from table 3.1 and table 3.2 the plant transfer function can be calculated as follows:

$$K_p = \frac{v_o}{LC_{pv}} = \frac{48}{1.559e^{-4} x\ 1.015x10^{-4}} = 79x10^8 \tag{4.29}$$

$$a_p = \frac{1}{C_{pv}R_{pv}} = \frac{1}{1.015x10^{-4}x9.6} = 1.04167x10^3 \tag{4.30}$$

$$b_p = \frac{1}{LC_{pv}} = \frac{1}{1.559e^{-4}x1.015x10^{-4}} = 6.414x10^7 \tag{4.31}$$

Finally the transfer function of linearized plant model will be:

$$G_p(s) = \frac{k_p}{s^2 + a_p s + b_p} = \frac{79x10^8}{s^2 + 1.04167x10^3\ s + 6.414x10^7} \tag{4.32}$$

In equation (3.84) the characteristics equation in its denominator has a form of

$$s^2 + 2\zeta w_n s + w_n^2 = s^2 + 1.04167x10^3\ s + 6.414x10^7 \tag{4.33}$$

The natural frequency (w_n) can be calculated as:

$$w_n^2 = 6.414x10^7$$

$$w_n = 8008.745$$

The target is to make an overall system have to be critically damped. This damping behavior is determined by damping ratio (ζ).when,

$\zeta < 1$ the system will be under damped.

$\zeta = 1$the system will be critically damped.

$\zeta = 0$ the system will be undamped

$\zeta > 1$the system will be over damped.

$$G_m(s) = \frac{y_p(s)}{u_c(s)} = \frac{k_m}{s^2 + a_m s + b_m} \quad (4.33)$$

By making $\zeta=1$, to making the system critical damped

$$a_m = 2\zeta w_n = 2x1x8008.745 = 16.0175x10^3 \quad (4.34)$$

$$b_m = b_p = 6.414x10^7 \quad (4.35)$$

$$G_m(s) = \frac{k_m}{s^2 + a_m s + b_m} = \frac{79x10^8}{s^2 + 16.0175x10^3\, s + 6.41x10^7} \quad (4.36)$$

By substituting the equations (4.32) and (4.36) in model which is represented in figure 3.20 and implementing the adaptation mechanisms formulated in (4.26) the MRAC is modeled as shown in figure below. The input for adaptive controller is duty cycle from the Ripple correlation controller. The duty cycle which is the output of the MRAC and input to the plant is used to maintain the system behavior to be critically damped.

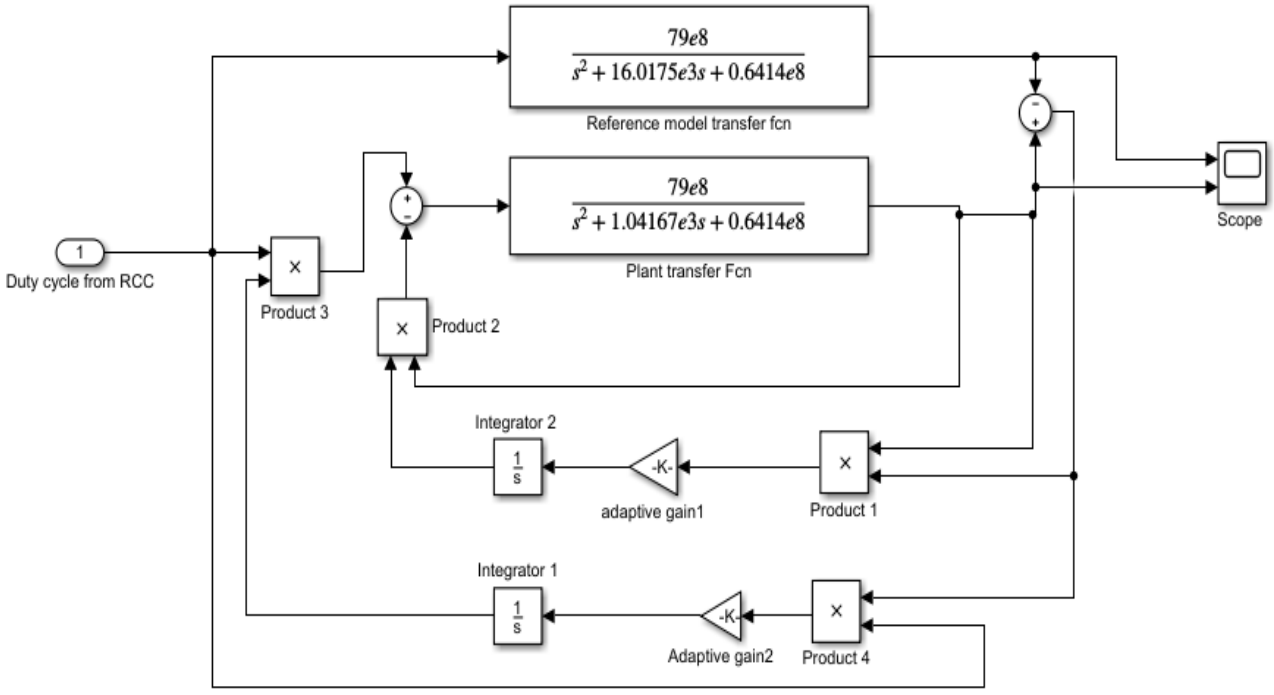

Figure 4.3: Simulink model of Model reference adaptive controller(MRAC) structure.

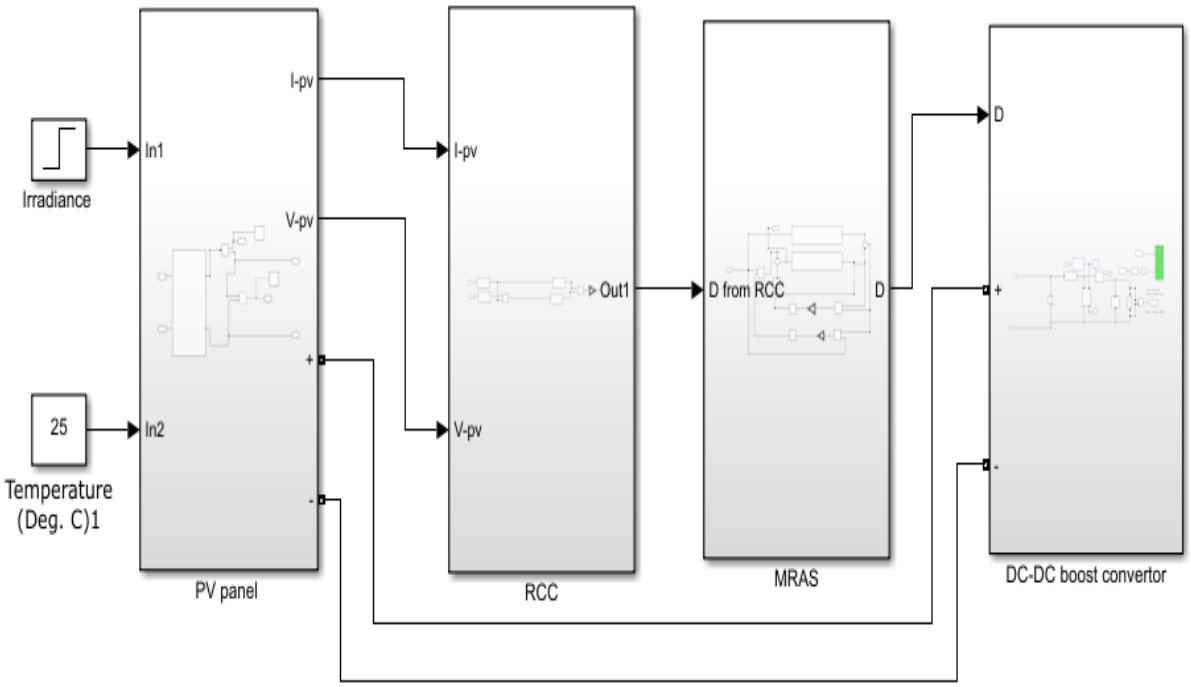

Figure 4.4: Simulink model of overall proposed system

CHAPTER FIVE

SIMULATION RESULTS AND DISCUSSIONS

5.1 Overview

In this chapter simulation result and discussion is presented. First, the simulation result for the PV module is discussed. Then the result of The DC_DC boost converter is presented. Finally, the simulation result of the system with RCC and MRAC presented and compared.

5.2 Simulation of PV module

The irradiation and temperature are two main factors, which strongly affect the characteristics of the PV module. The variation of one or both of them can vary the Maximum power point of the solar modules.

5.2.1 The simulation of the PV module at various irradiance level

In this simulation, the irradiance was varied from 400w/m^2, 600 w/m^2, and 1000 w/m^2, and the temperature was held constant at 25^{0}C. The result in figure 4.1 and figure 4.2 shows the power-voltage curve and current-voltage curve respectively.

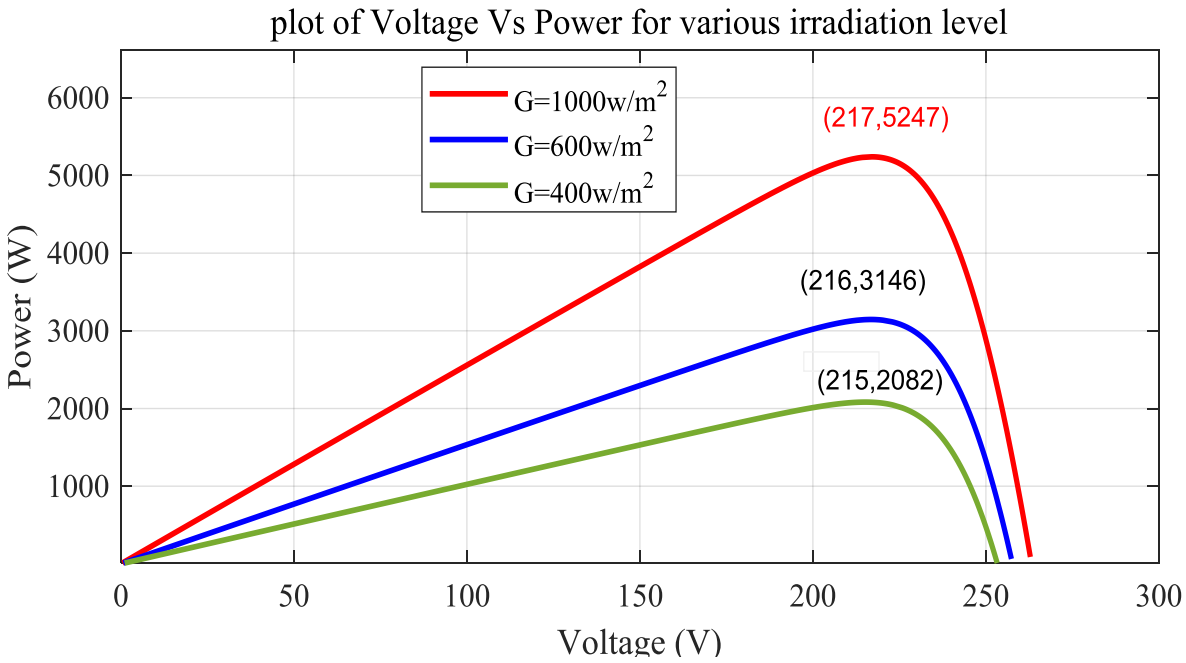

Figure 5.1: Simulation result of PV model for various radiations (V-P curve at a constant temperature, T=25^{o}c)

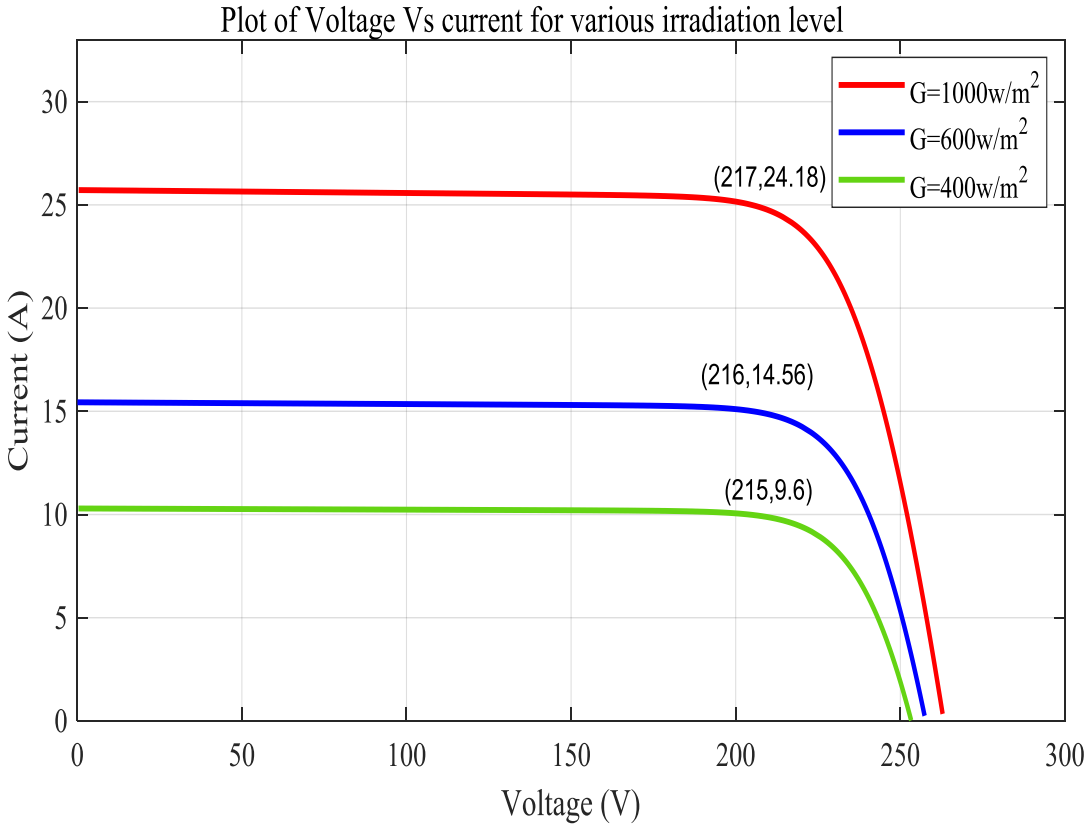

Figure 5.2: Simulation result of PV model for various radiations (V-I curve at a constant temperature, T=25^{o}c)

As explained previously in equation (3.1), the photocurrent has a direct relation to the solar irradiation, therefore an increase in irradiance level yields high photocurrent. Since the PV current mainly depends on the photocurrent as shown in equation (3.5) the so, increasing the irradiation level increases the PV current. Due to this factor, the voltage-current characteristic varies with the irradiation. As shown in figure 5.2, the irradiance mostly affects the current. The irradiation effect on both the current and voltage is positive. Due to this the effect on the power is also positive: the more irradiation, the more power is generated as shown in figure 5.1.

4.2.2 The simulation of the PV module at a various temperature level

In this simulation, the temperature was set at three different values such as 25^{0}C, 50^{0}C, and 75^{0}C and the irradiation was adjusted at G=1000w/m^{2}. The power-voltage curve and current-voltage curve were shown in figure 5.3 and figure 5.4 respectively.

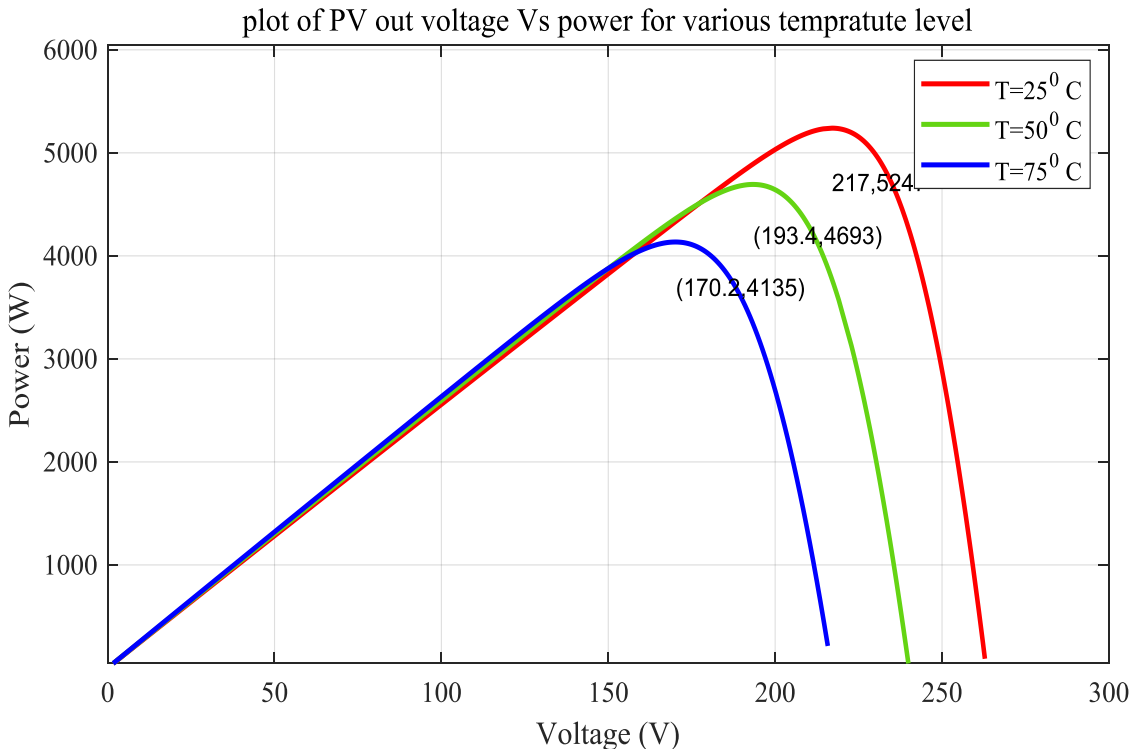

Figure 5.3: Simulation result of PV model for various temperatures (V-P curve at constant irradiance, G=1000w/m^2)

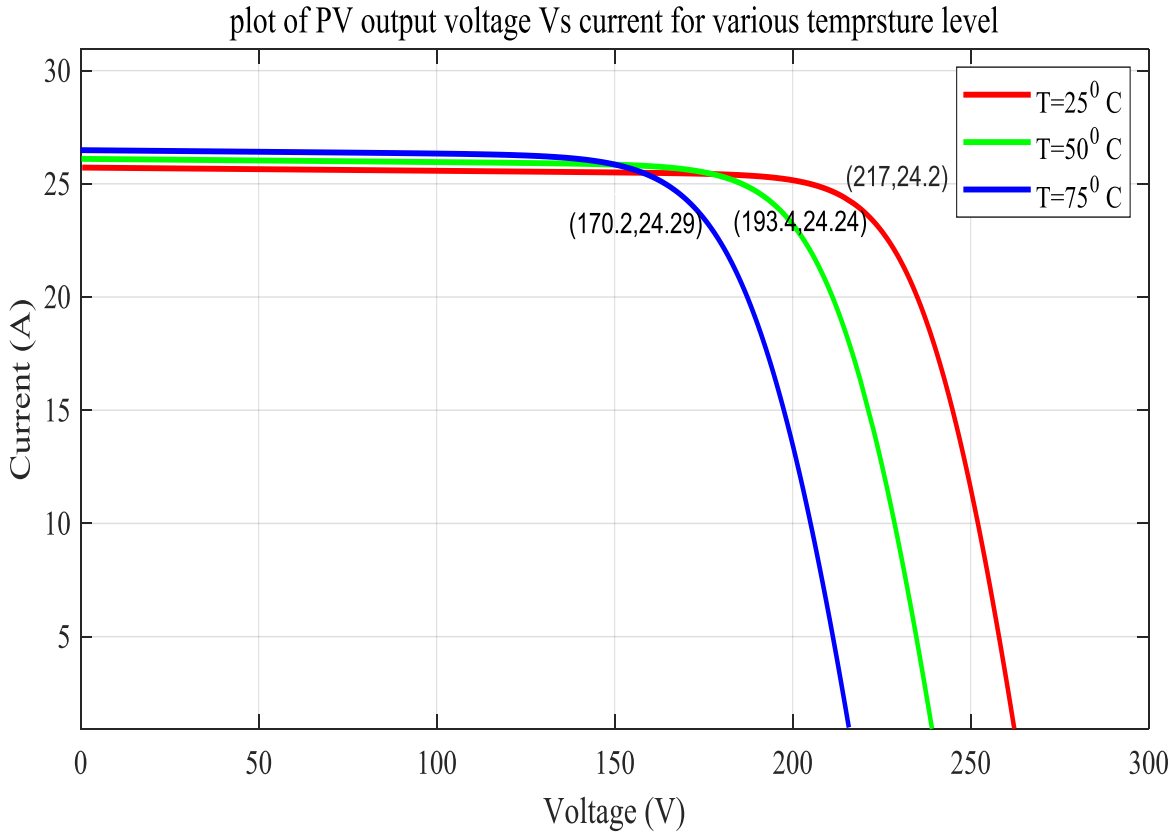

Figure 5.4: Simulation result of PV model for various temperatures (V-I curve at constant irradiance, G=1000w/m^2)

From the simulation result of figure 5.4 as the temperature increases the PV voltage decrease. There is a little increment in the PV current. The increase in current when temperature increase is very slight and it is not able compensate for the reduction of voltage resulted due to an increase in temperature. That is the reason for decreasing power as shown in the simulation result in figure 5.3. Generally from the results of simulation, it is observed that with variation of irradiance and temperature there is a variation of maximum power point.

5.3 Simulation of DC-DC boost converter

In this simulation, the duty cycle and input voltage were varied for the parameter values in table 3.2. The simulation results are shown figure below.

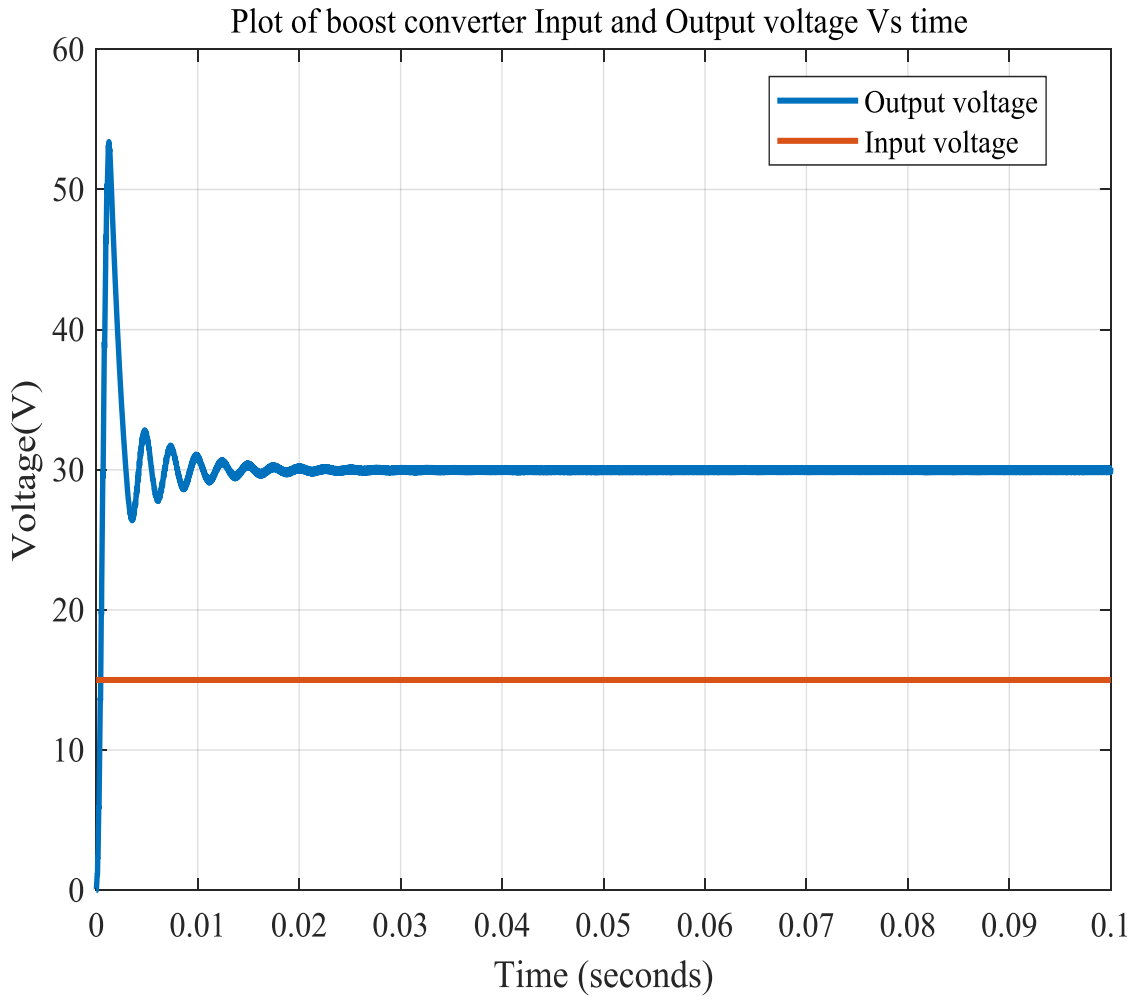

Figure 5.5: Simulation result of DC-DCboost converter for duty cycle D =0.5 and v_{in}=15V

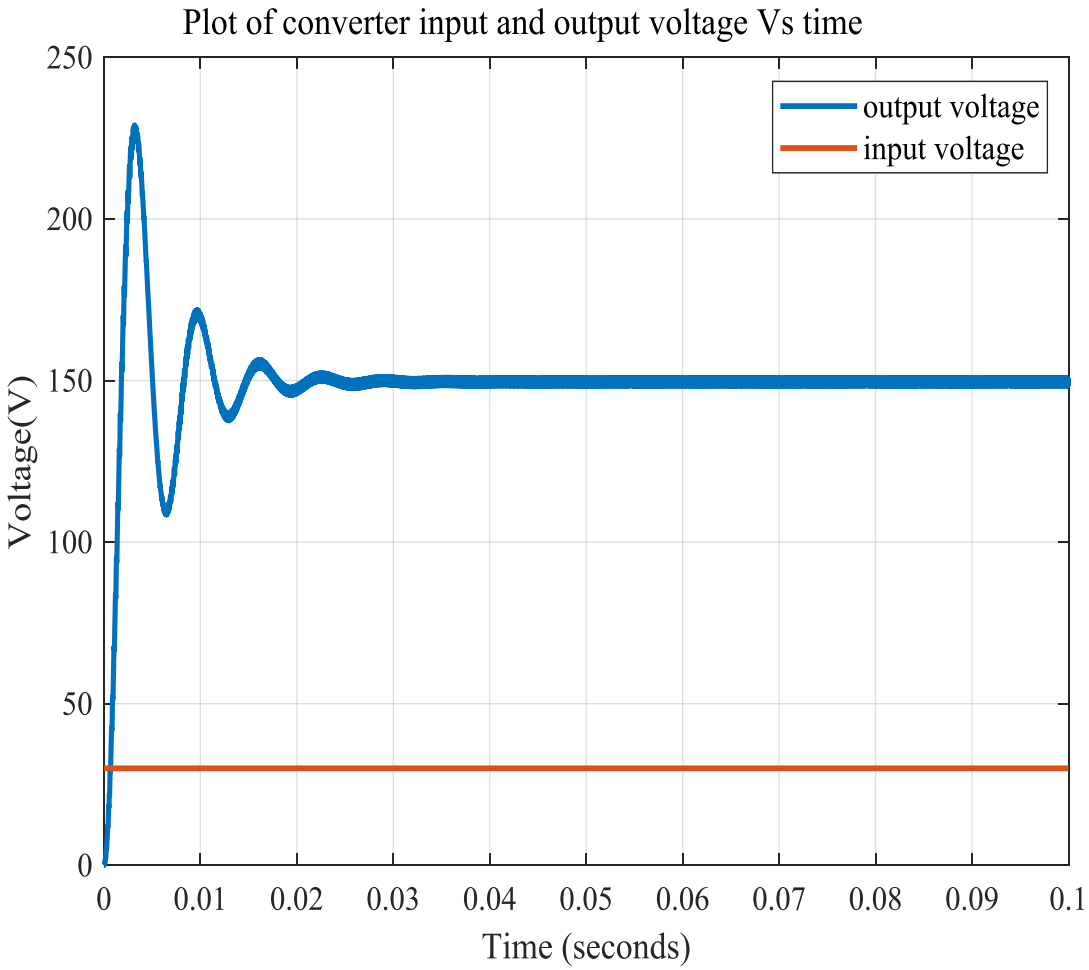

Figure 5.6: Simulation result of DC-DCboost converter for duty cycle D=0.8 and v_{in}=30V

The simulation is done for duty cycles of D=0.5 and for D=0.8. From the results obtained it is observed that converter output is 30 V for a duty cycle of D=0.5 for an input voltage of 15 V, and the output voltage is 150V for the duty cycle of D=0.8 for an input voltage of 30V. From the results obtained, it is observed that the boost converter steps up the voltage from 15V to 30V and 30V to 150V as shown in figure 5.5 and figure 5.6 respectively per the parameters derived earlier and satisfies the relationship rule of duty ratio, input and output voltage.

5.4 Simulation of Ripple correlation control

The ripple correlation control uses inherent ripples available in power electronics which is produced during the switching period.

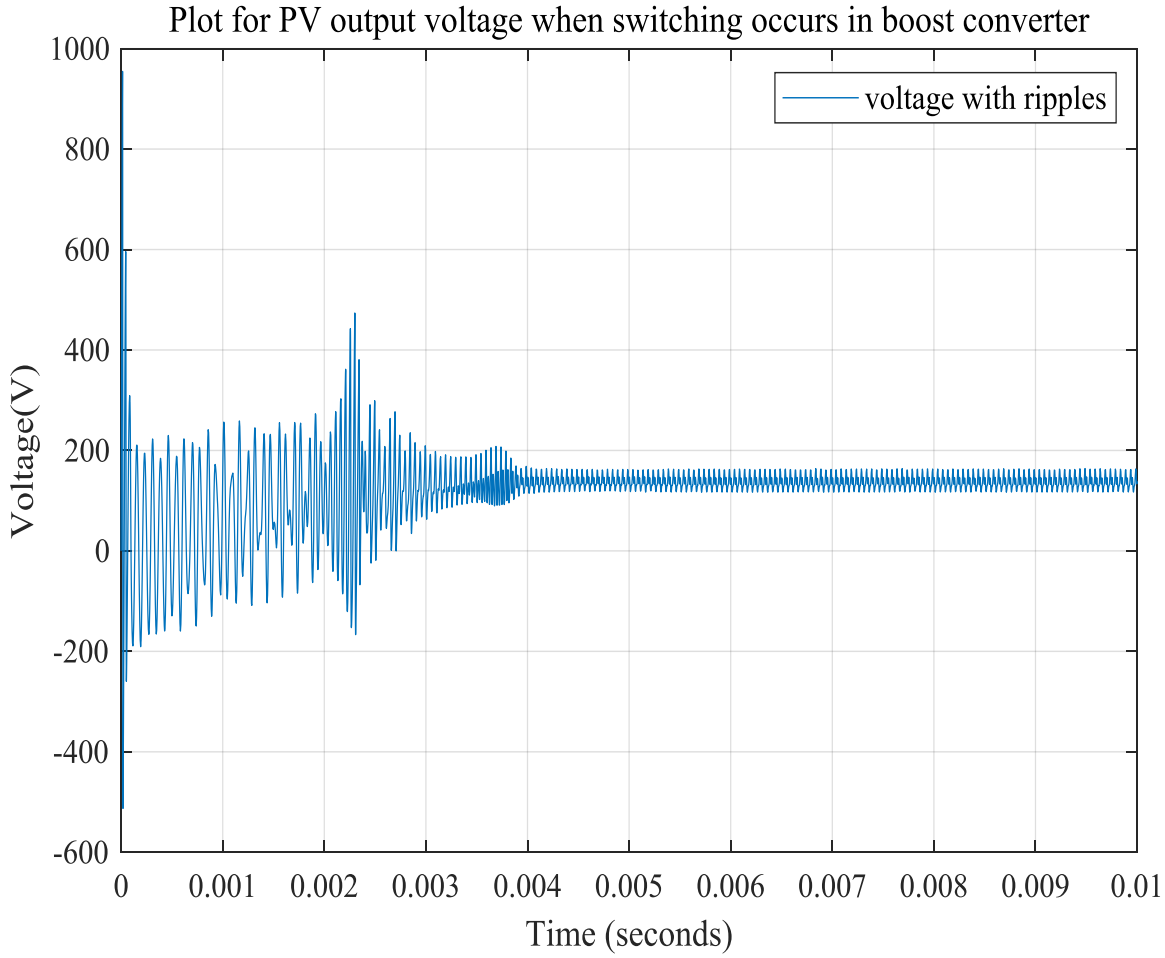

Figure 5.7: Simulation result of PV voltage with ripples.

The simulation was carried out by connecting the PV output voltage to the DC-DC boost converter. From the observed simulation result shown in figure 5.7, there is a ripple on the PV output voltage. These ripples will be used for obtaining the duty cycle for maximum power point. In the ripple correlation technique, these ripples are utilized as input to the Ripple correlation controller.

5.4.1 Simulation of the DC-DC boost converter with the PV system and MPPT controller

In this section, the simulation of the ripple correlation controller, which is the MPPT controller, with PV module and boost converter was discussed in detail. Various irradiance levels are used for the simulation.

5.4.1.1 Simulation of Photovoltaic voltage (Vpv), current (Ipv) and power (Ppv)

The simulation is set to run for t=0s to 0.1 s and the solar irradiance is set at G=1000w/m^2

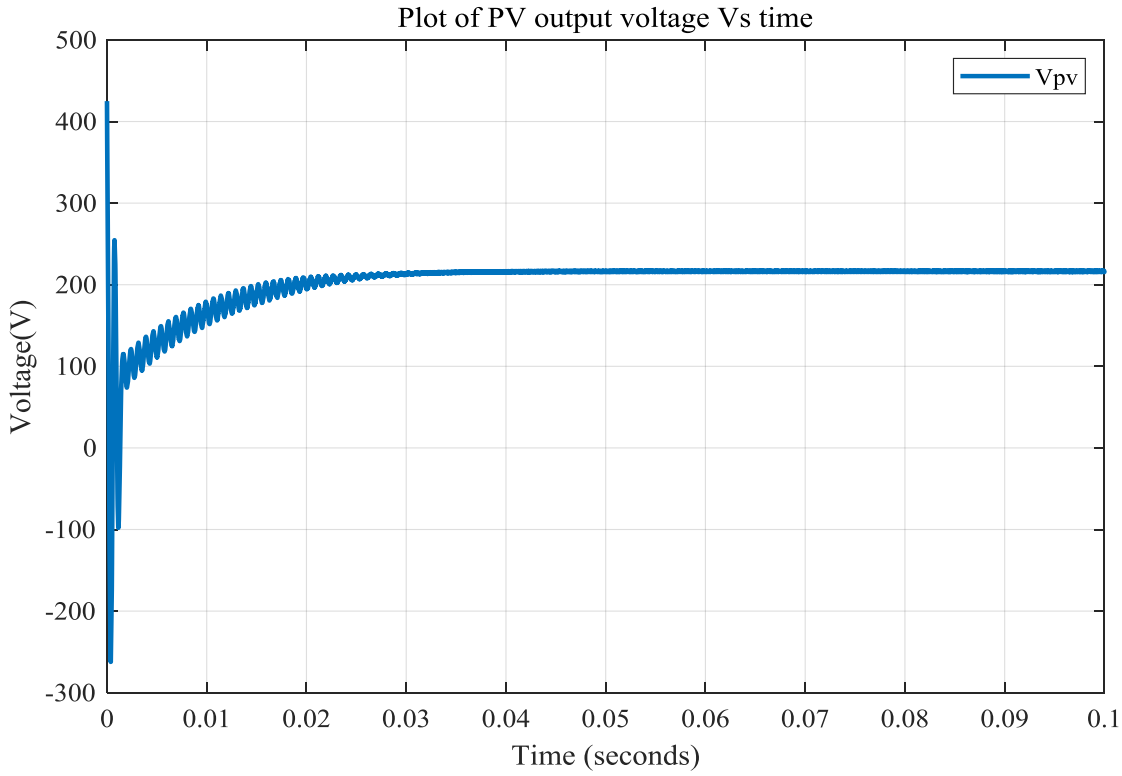

Figure 5.8: Simulation result for photovoltaic output voltage (Vpv) at 1000w/m^2 when RCC used as MPPT controller

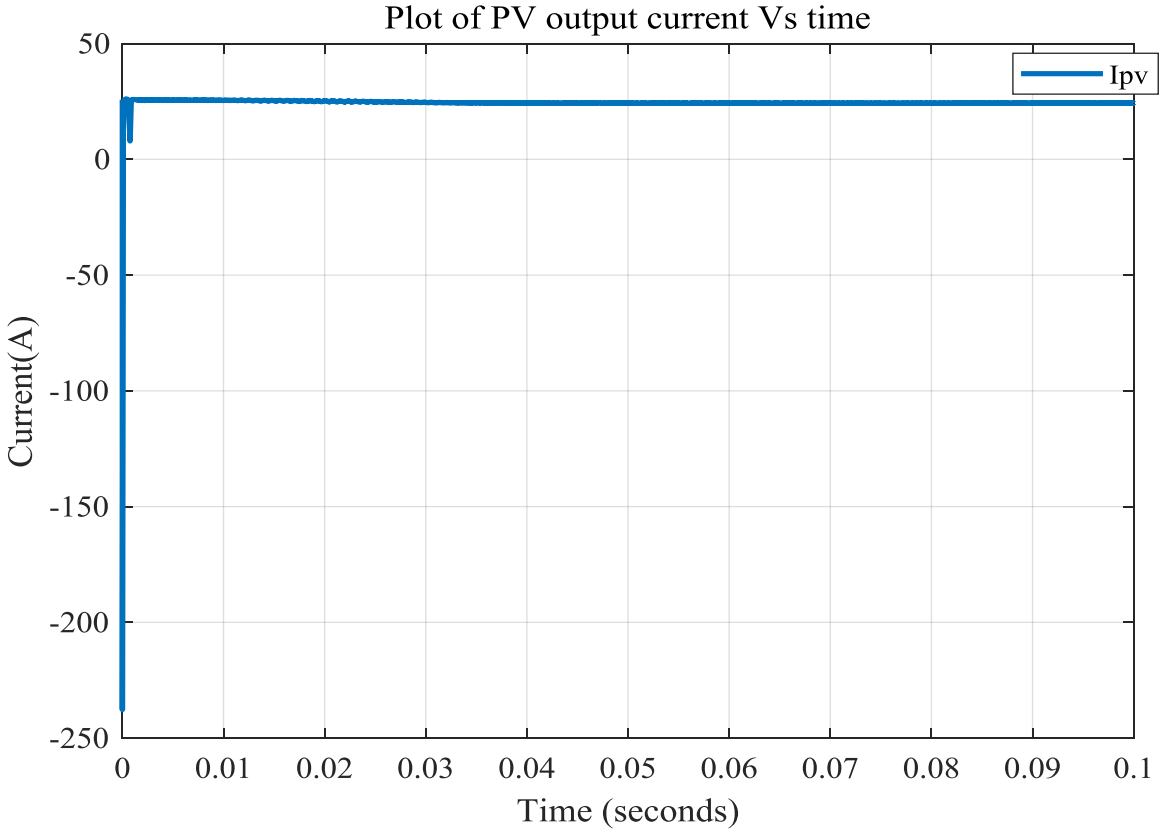

Figure 5.9: Simulation result for photovoltaic output current (Ipv) at 1000w/m^2 when RCC used as MPPT controller

In figure 5.8 the output voltage of the PV array is 217 V at t=0.1s when the irradiance is 1000w/m^2, i.e. V_{pv}max=217 V. As it is seen from figure 5.8 the photovoltaic output voltage shows oscillation when it is going to attain maximum value and it goes to settle slowly or goes slowly to steady-state. From figure 5.9 the Photovoltaic output current I_{pv} reaches steady state rapidly than V_{PV}. The maximum current output I_{pv}max is 24.34A at t=0.1s.

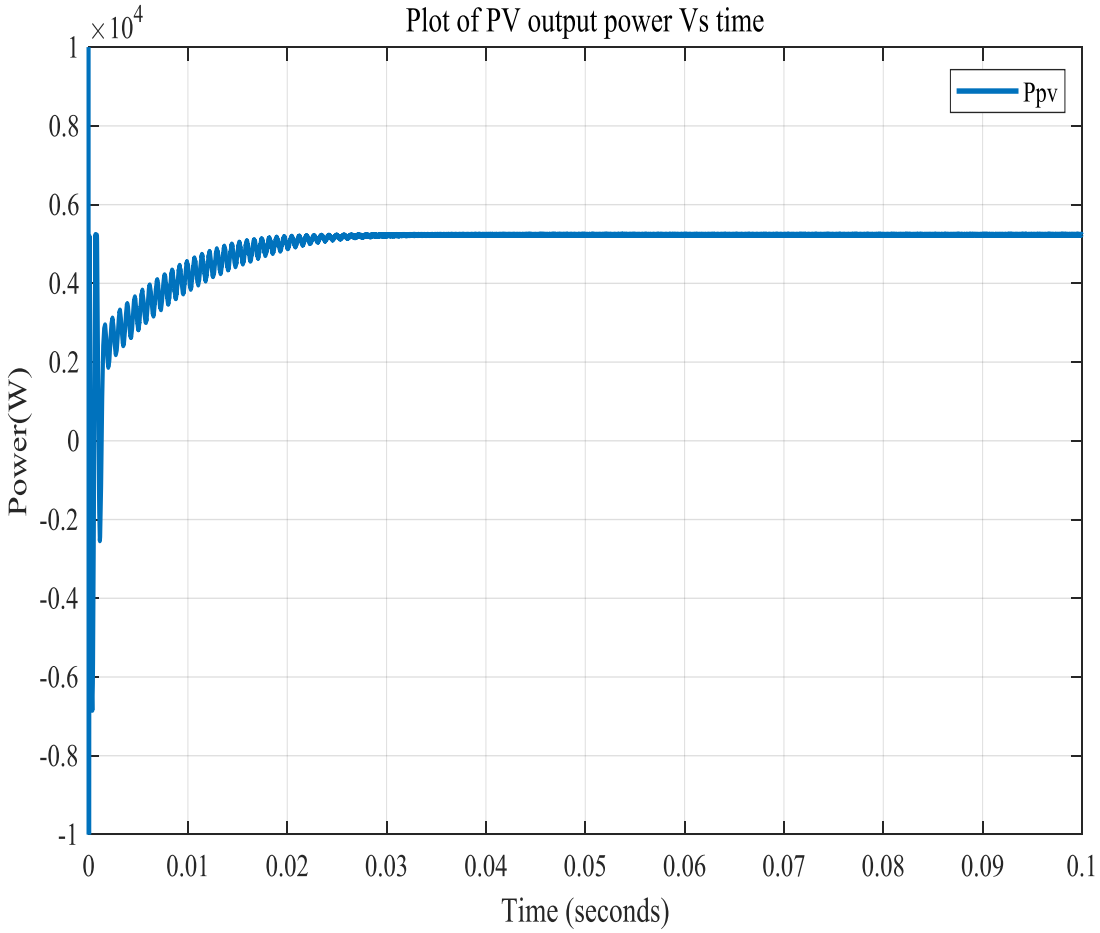

Figure 5.10: Simulation result for photovoltaic output power (Ppv) at 1000w/$m^2$when RCC used as MPPT controller.

Form figure 5.10 the power at 5237 Watt is the maximum power of the PV array under 1000 W/m^2 irradiance which is observed at t=0.1s. The RCC can track the MPP quickly. The power also oscillates around the MPP and goes to steady-state slowly like V_{pv}.

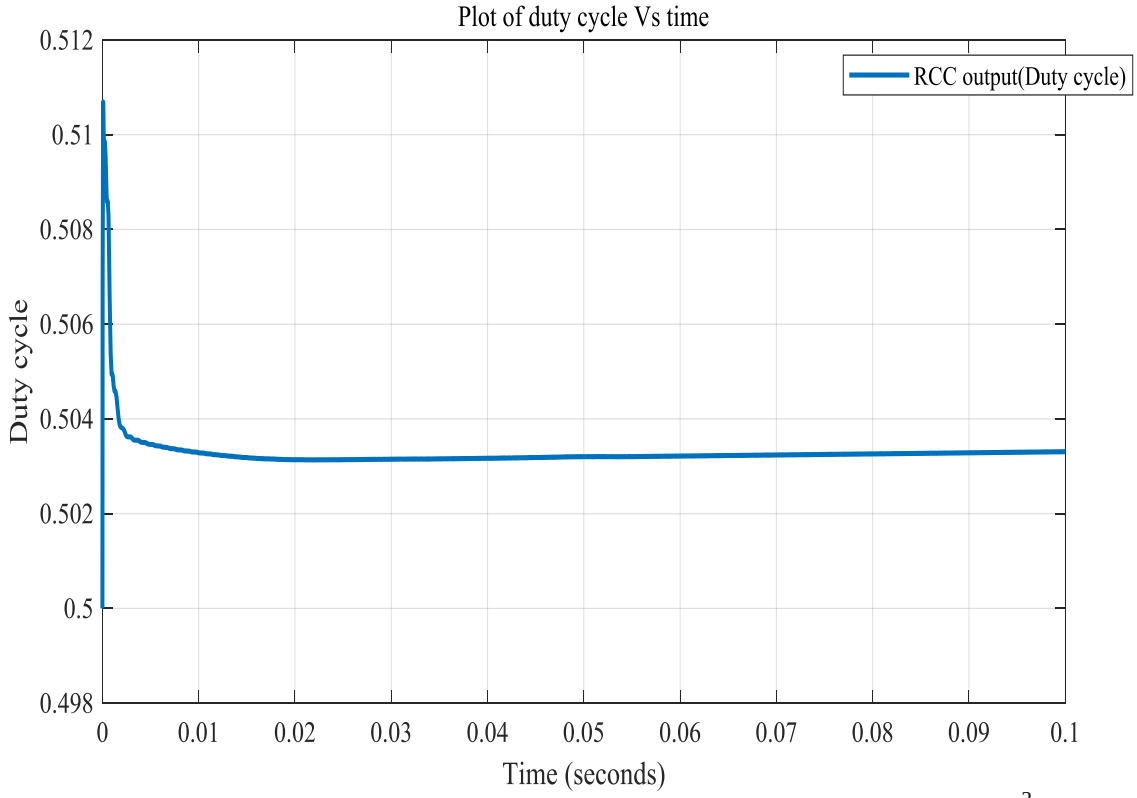

Figure 5.11: Simulation result for MPPT controller output (duty cycle) at 1000w/m^2 when RCC used as MPPT controller.

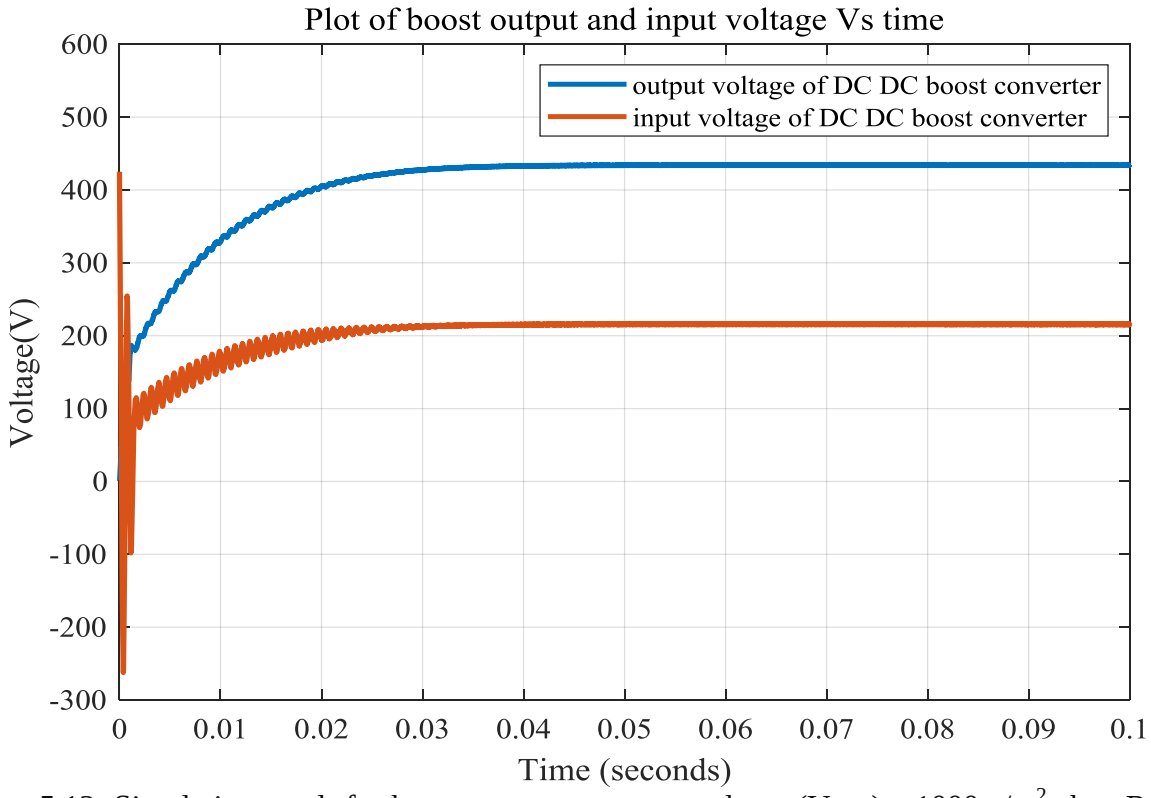

Figure 5.12: Simulation result for boost converter output voltage (Vout)at 1000w/m^{2}when RCC used as MPPT controller.

From the simulation result shown in figure 5.11 the MPPT controller is searching for the duty cycle for maximum power point. It observed that the MPPT controller rapidly attained the duty cycle for MPP. The duty cycle attained by the MPPT controller for irradiance of 1000w/m^2 is 0.5033. This will be the input to the DC-DC boost converter.

The same procedure is also used to examine the performance of the DC-DC boost converter. Figure 5.12 shows the input voltage (Vpv) and output voltage (Vout) the boost converter. The boost converter boosts the input voltage from 217V to 434.6V which satisfies the relationship $V_o = \frac{V_{in}}{(1-D)} = \frac{217}{(1-0.5033)} = 434.6V$.

Similarly, the simulation is done for G=2000w/m^2. The simulation result is shown in the following figures.

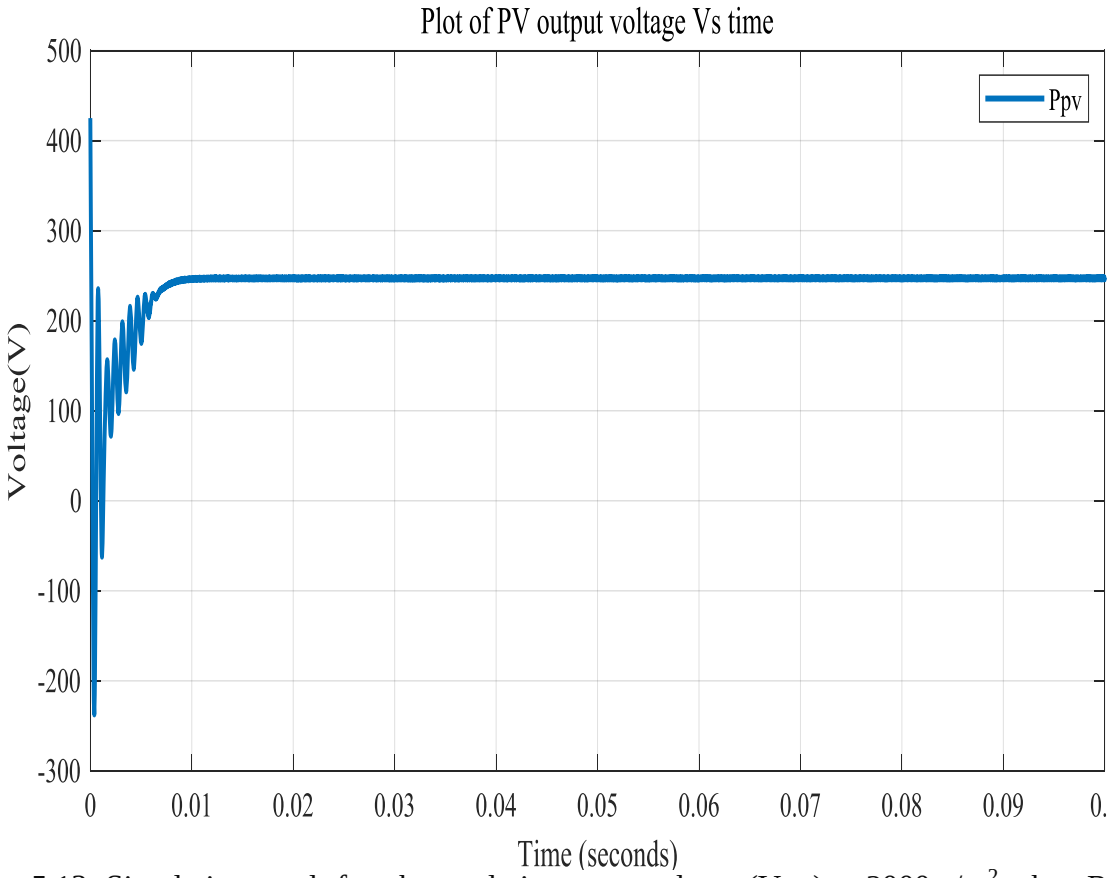

Figure 5.13: Simulation result for photovoltaic output voltage (Vpv) at 2000w/m^2 when RCC is used as the MPPT controller.

In figure 5.13 the photovoltaic array output voltage is 248.2 V at t=0.1s when the irradiance is 2000w/m^2, i.e. V_{pv}max=248.2V. As it is observed from figure 5.13 the photovoltaic output voltage similarly shows oscillation and it is going to settle slowly or goes slowly to steady-state

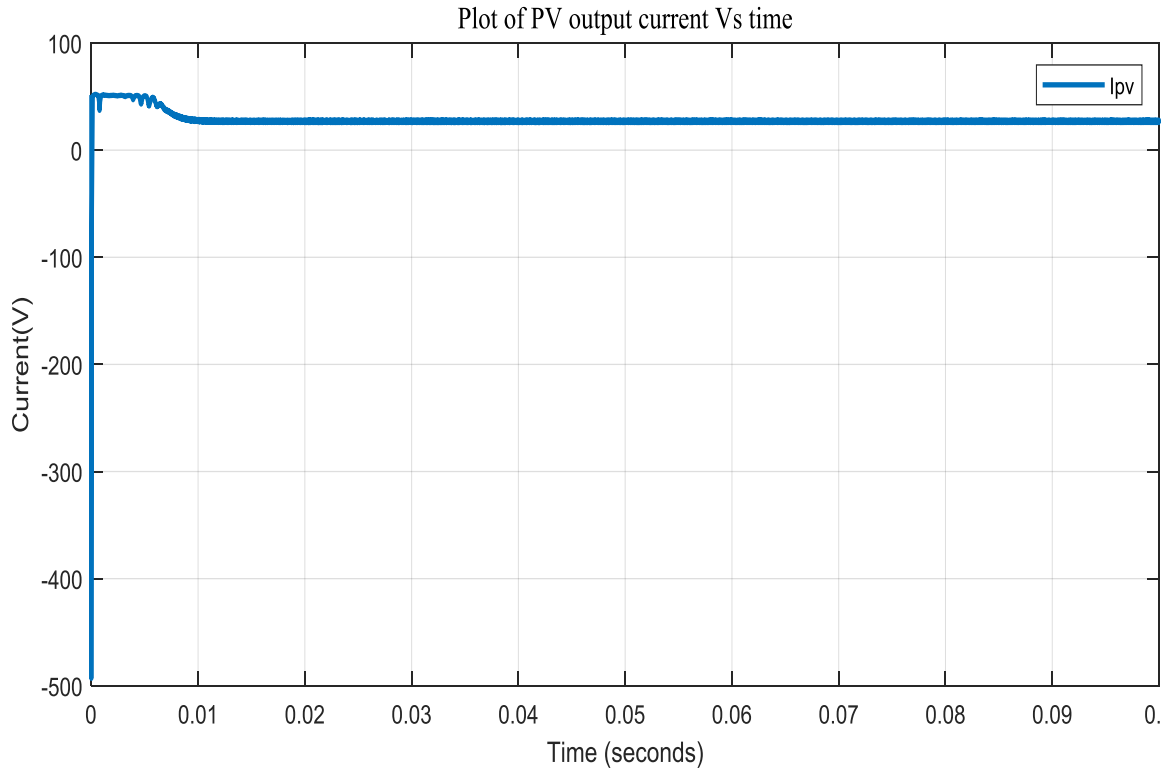

Figure 5.14: Simulation result for photovoltaic output current (Ipv) at 2000w/m^2 when RCC is used as the MPPT controller.

In a similar manner as shown in simulation of 1000w/m^2 the current reaches steady state rapidly. From figure 5.14 maximum current is, I_{pv}max=28.6A at t =0.1s.

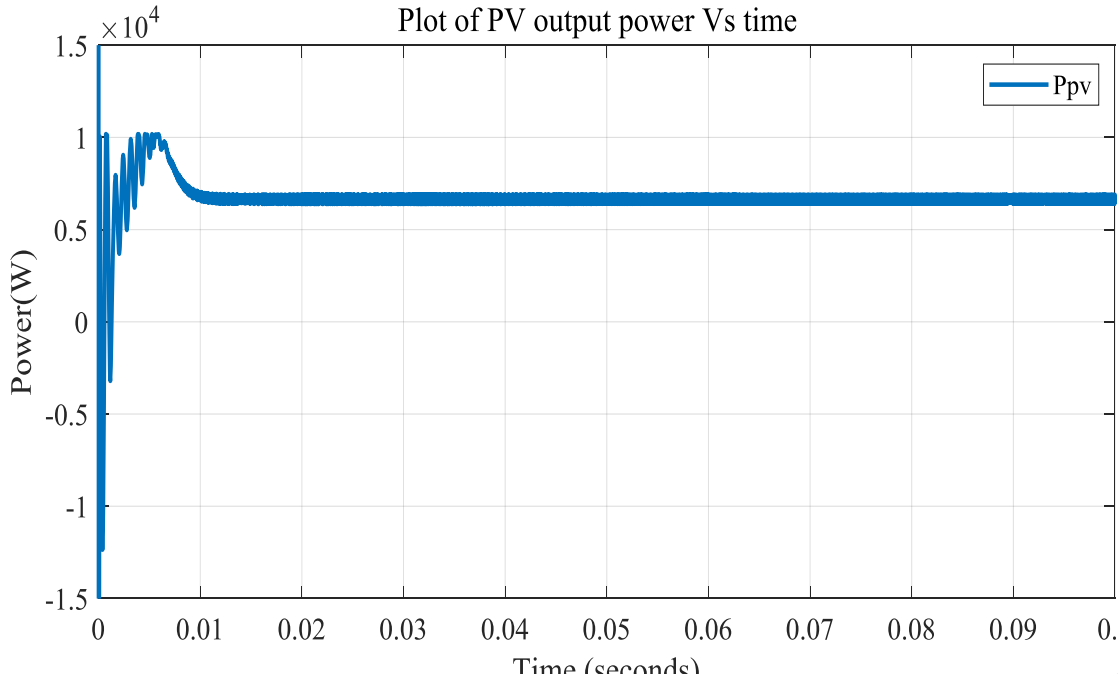

Figure 5.15: Simulation result for photovoltaic output power (P_{pv}) at 2000w/m when RCC is used as MPPT controller.

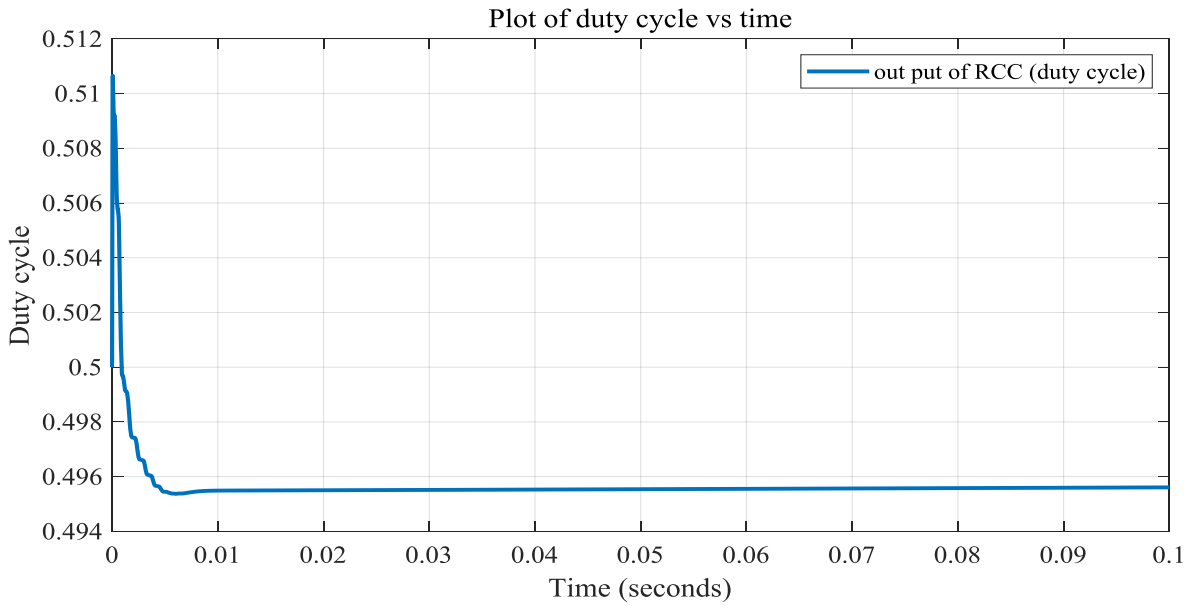

Figure 5.16: Simulation result for MPPT controller output (duty cycle) at 2000w/m^2 when RCC is used as the MPPT controller.

Form figure 5.15 the power at 6887Watt, which is (p=Vpv. Ipv), is the maximum power of the PV under 2000W/m^2 irradiance which is observed at t=0.1s. The MPPT controller can track the maximum power almost immediately. From figure 5.15 it also observed that the MPPT controller rapidly attained the duty cycle for MPP. The duty cycle attained by the MPPT controller for irradiance of 2000w/m^2 is 0.4956.

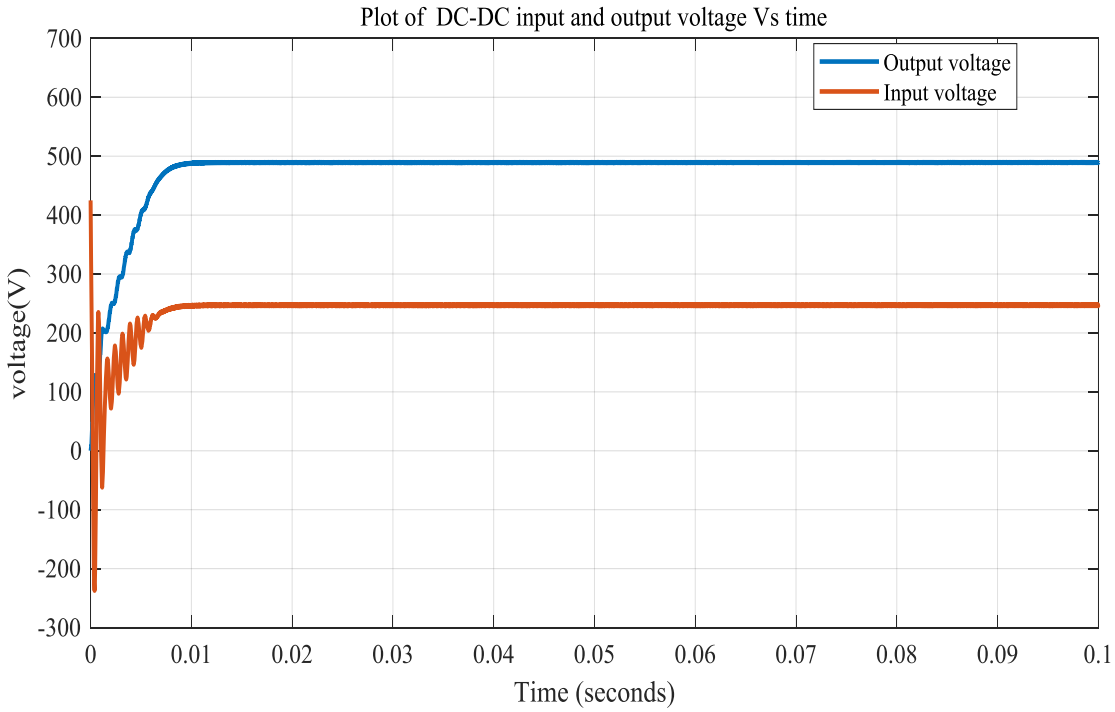

Figure 5.17: Simulation result for boost converter output voltage (Vout) at 2000w/m^{2}when RCC is used as the MPPT controller.

In a similar way, the simulation is also done for 2000w/m^2 to check the performance of the DC-DC boost converter. Figure 5.17 shows the input voltage (Vpv) and output voltage (Vout) of the boost converter. The DC-DC boost converter increases the input from 248.2 V to 492V that satisfies the relation $V_o = \frac{V_{in}}{(1-D)} = \frac{248.2}{(1-0.4956)} = 492$ V.

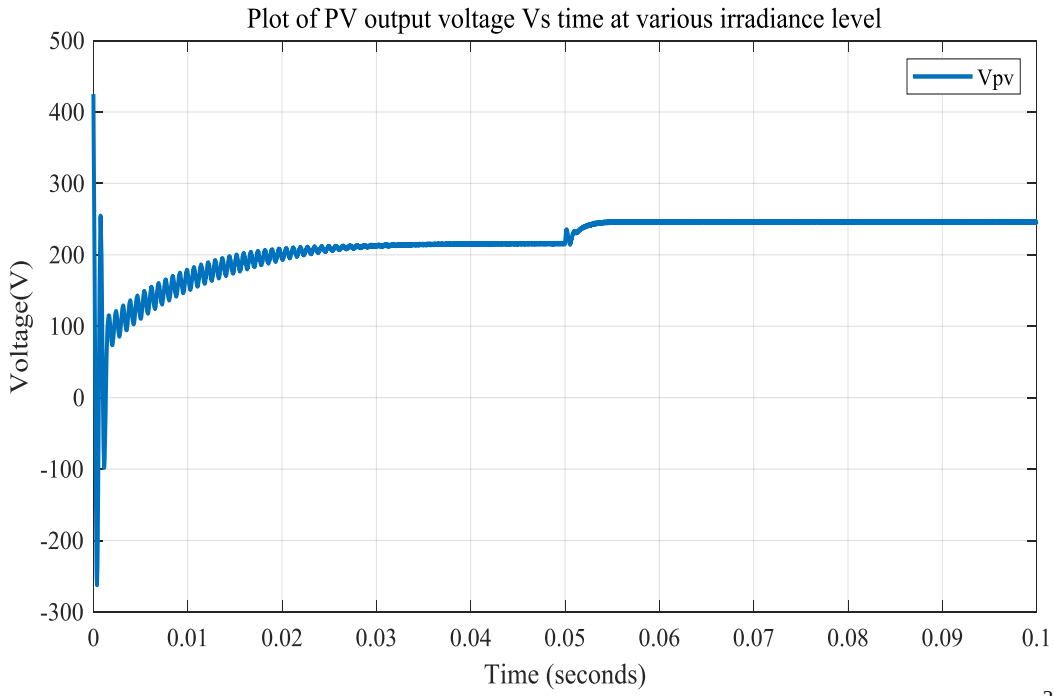

Figure 5.18: Simulation result of photovoltaic output voltage (Vpv) at G=1000 w/m^2 and G = 2000w/ m^2 when RCC is used as the MPPT controller.

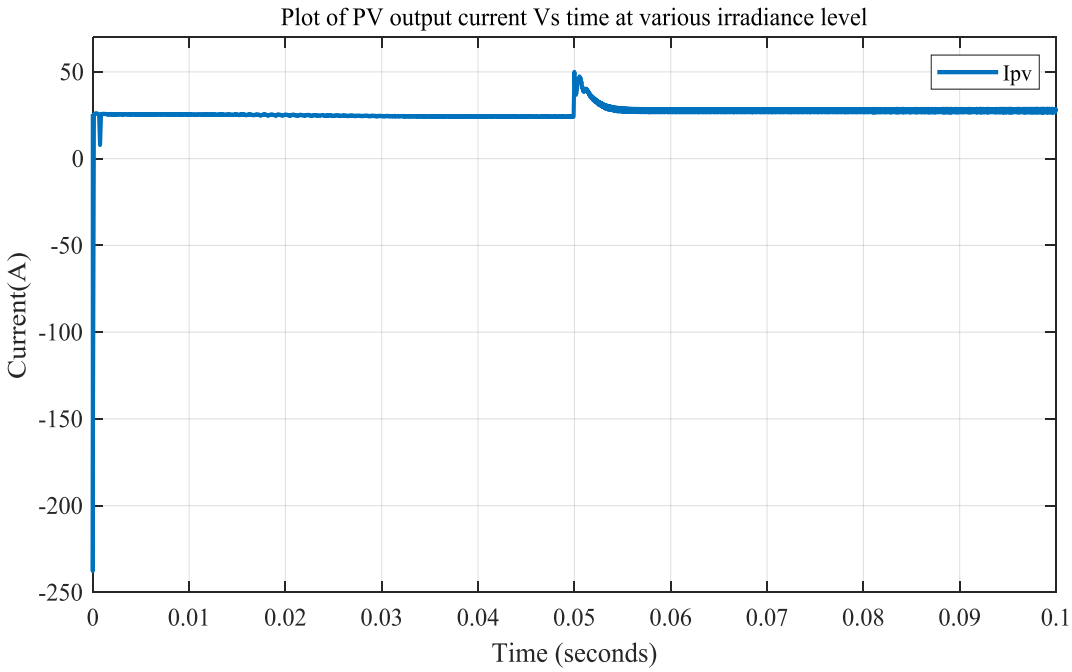

Figure 5.19: Simulation result for photovoltaic output current (Ipv) at G=1000 w/m^2 and G = 2000w/ m^2 when RCC is used as the MPPT controller.

Figure 5.18 shows the output voltage of the PV array. The simulation was run for t=0s to 0.2 s. Initially, the solar irradiance is adjusted at G=1000 w/m^2, and at t=0.1s irradiation was changed to 2000 w/m^2. During this time the system goes to a new MPP. The maximum PV output voltage varies from 217 V to 248.2 V. From figure 5.19 also shows the PV output current varies from 24.34A to 28.6 A.

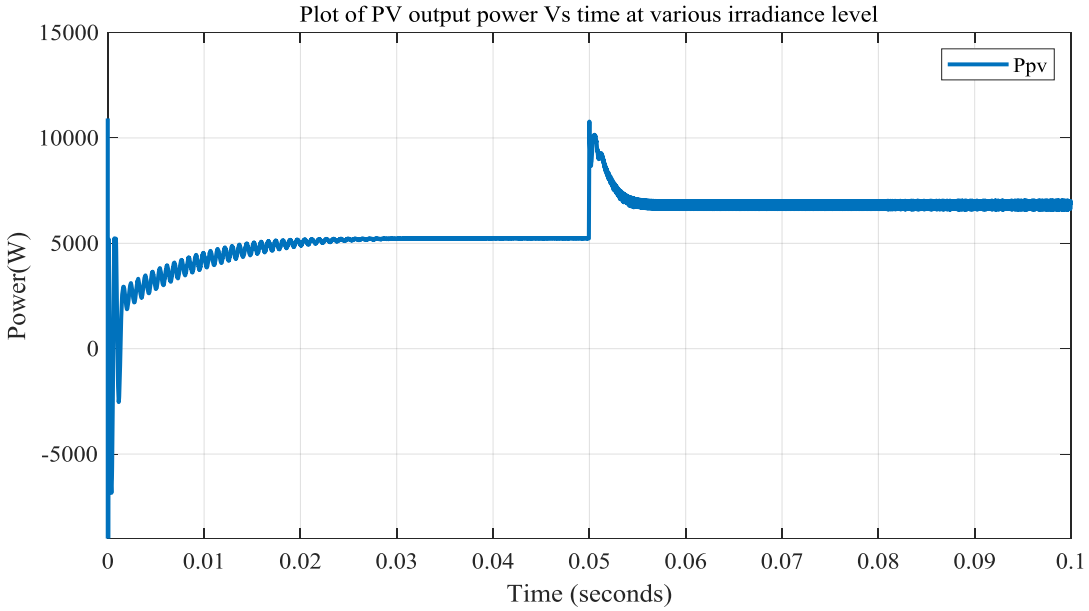

Figure 4.20: Simulation result for photovoltaic output power (P_{pv}) at G=1000 w/m^2 and G = 2000w/ m^2 when RCC is used as the MPPT controller.

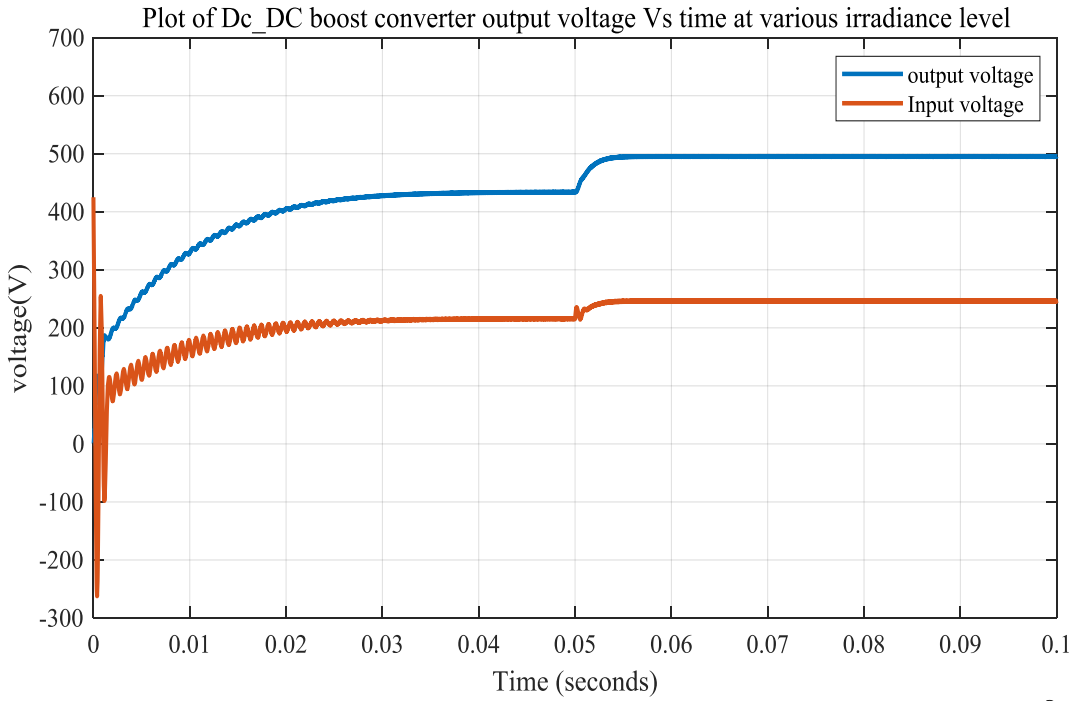

Figure 5.21: Simulation result for DC-DC boost output voltage (V_O) at G=1000 w/m^2 and G = 2000w/ m^2 for t=0.2s when RCC is used as the MPPT controller.

Figure 5.20 shows the simulation result for the photovoltaic output power (Ppv) at G=1000 w/m^2 and G = 2000w/m^2.The power, P_{pv}max=5237 watt for G=1000 w/m^2, and then the power goes to P_{pv}max=6887 watt for G=2000w/m^2.

The simulation is also done to check whether the DC-DC boost converter is performing properly or not. Figure 5.21 shows the input voltage (Vpv) and output voltage (Vout) of the boost converter. The boost converter boosts the input voltage from 217V to 434.6V for the duty cycle of 0.5033, and 248.2 V to 492V for the duty cycle of d=0.4956 that satisfies the relation Vo=Vpv/(1-d) for both irradiance levels. All the above simulation results show that the variation in irradiance changes MPP. If the irradiation increases the voltage increases and the duty cycle decreses.This shows the relationship between PV output voltage and the duty cycle in equation (3.20).

5.4.2 Simulation of DC-DC boost converter with the PV system, MPPT controller and MRAC.

In this section the simulation was done for the MRAC with the RCC and the result was discussed for both controllers. The simulation results for the MRAC were shown by using blue color and for the RCC were shown by using red color.

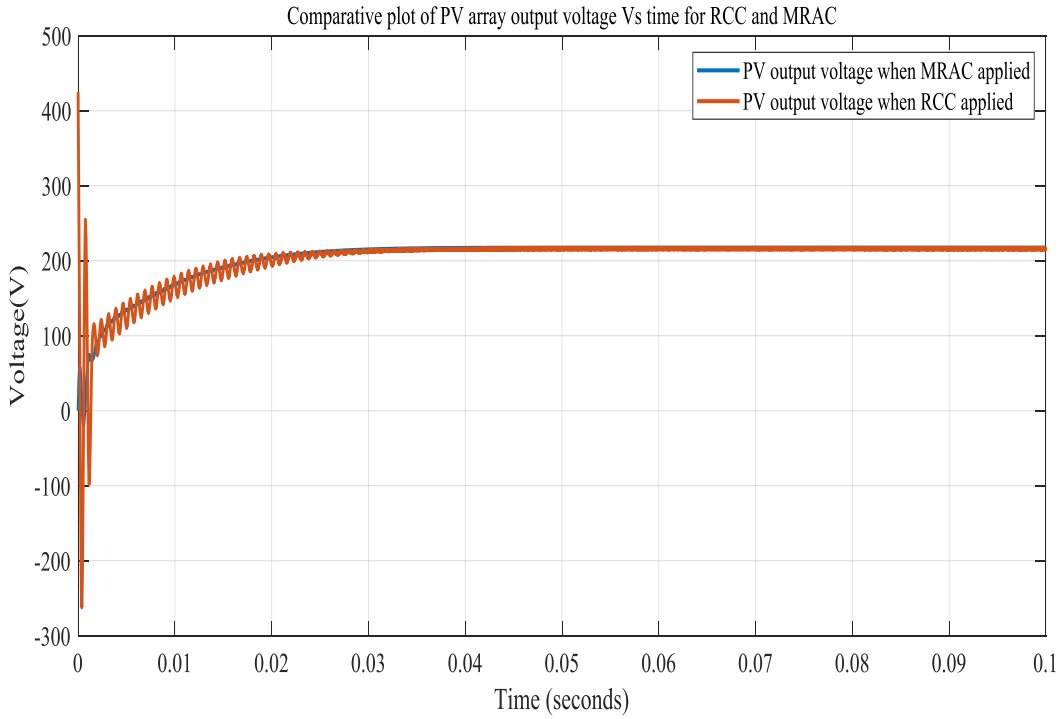

Figure 5.22: Simulation result for the photovoltaic output voltage (Vpv) at G=1000w/m^2

In a similar manner the simulation done for the MRAC for the time duration of t=0.1s. As shown figure 5.22 above the simulation result of ripple correlation controller is shown in red color and

the MRAC is shown in blue color. From the above simulation result it is observed that the photovoltaic voltage reaches its steady-state rapidly at t=0.025s and removes the oscillation at t=0.002s when the proposed controller, the MRAC, used. When the RCC is used there is an oscillation even at t=0.031s and reaches steady state at t=0.035s. This simulation result shows the proposed controller, the MRAC reduces the oscillation by reducing the settling time. The simulation result for the photovoltaic current is shown in figure 5.23. As it is observed from the figure, the result shows that the proposed controller, the MRAC removes the undershoot produced by the RCC.

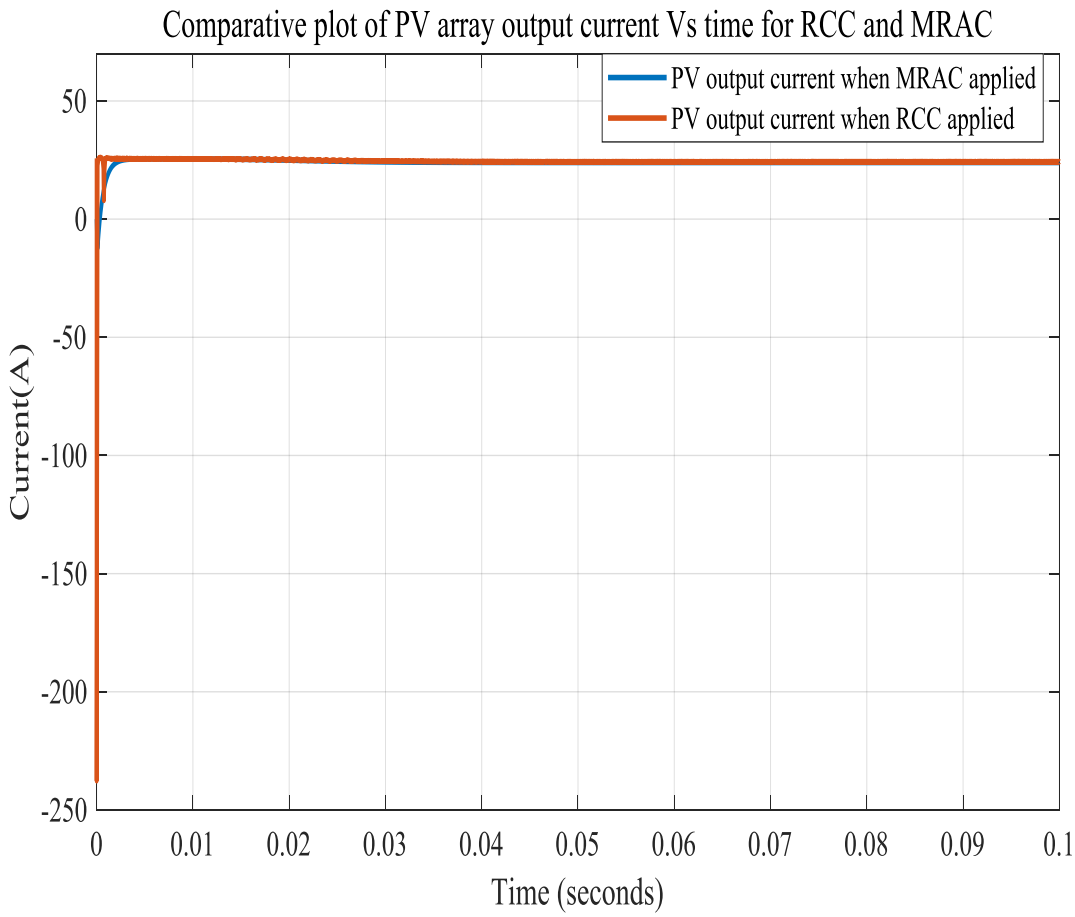

Figure 5.23: Simulation result for photovoltaic output current (Ipv) at G=1000w/m^2

From the simulation result shown in figure 5.24 below, it is observed that the photovoltaic power settles at its maximum power point at t=0.025s when the MRAC used. When the RCC is used there is an oscillation even at t=0.03s, and the power settles at t=0.031. This simulation result shows the MRAC reduces the oscillation and the settling time.

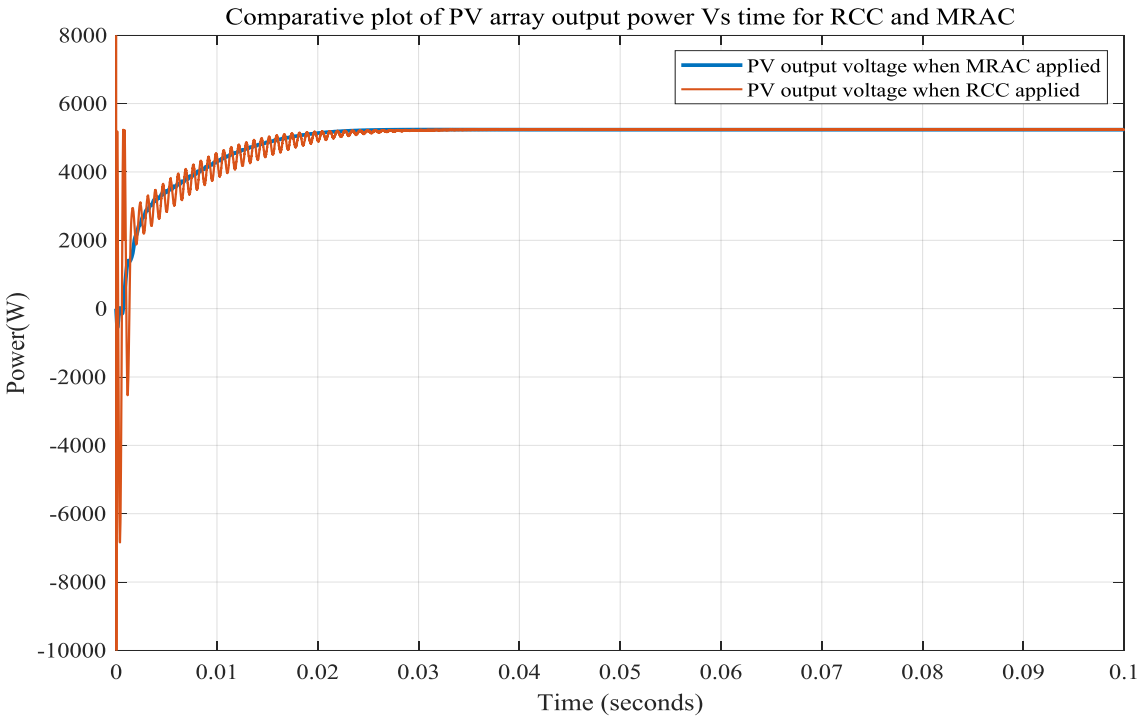

Figure 5.24: Simulation result for the photovoltaic output power (Ppv) at G=1000w/m^2

The irradiation is changed to 2000w/m^2 and the same procedure is used as done for irradiation at 1000w/m^2, and the simulation results were observed in the following section.

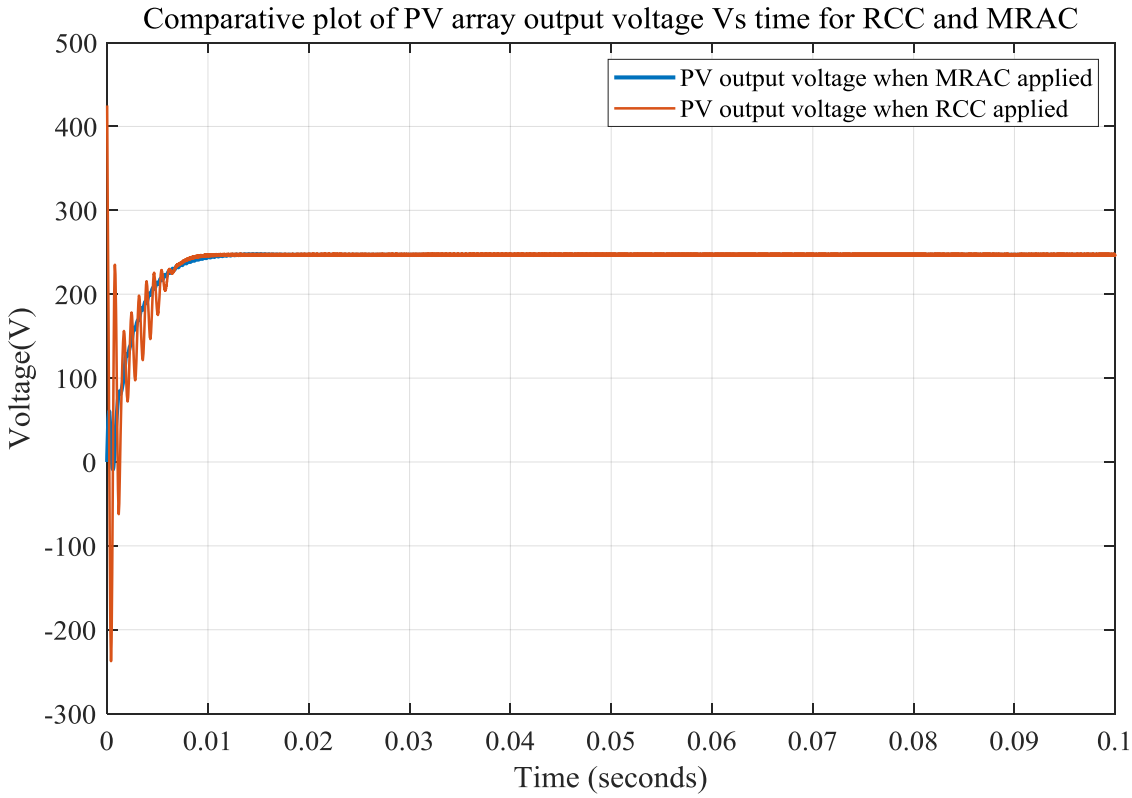

Figure 5.25: Simulation result for the photovoltaic output voltage (Vpv) at 2000w/m^2

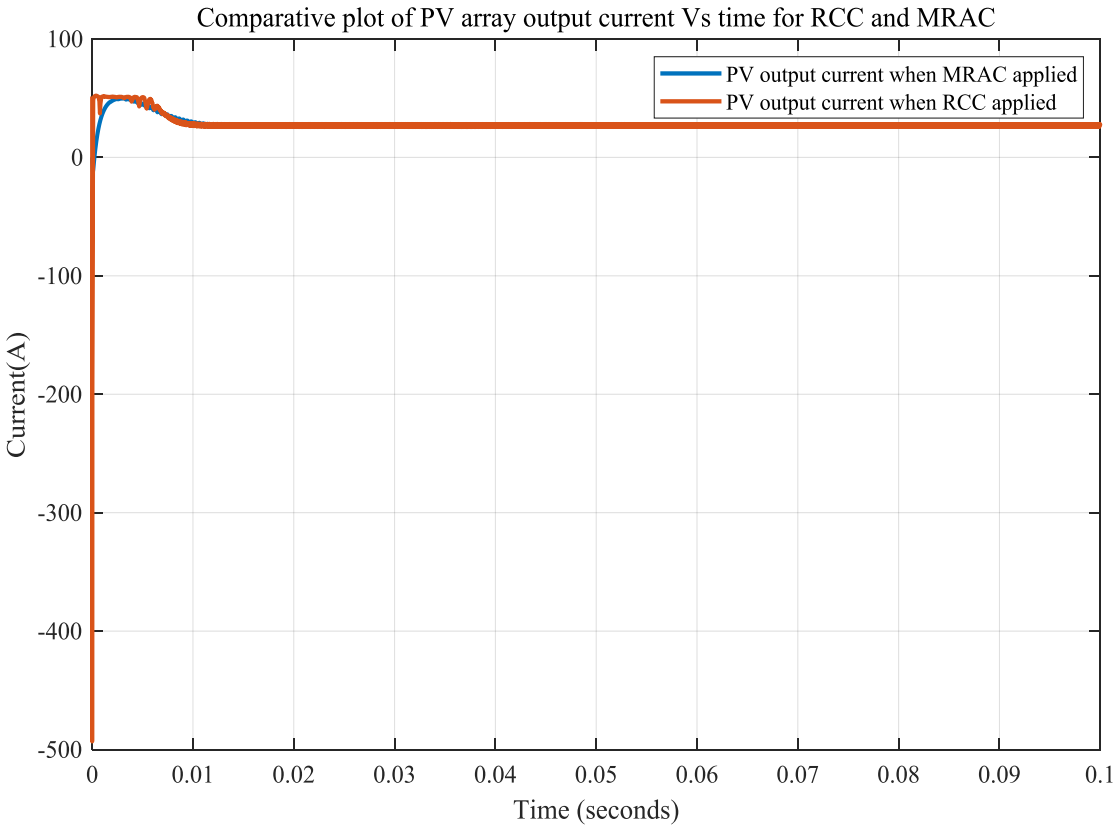

Figure 5.26: Simulation result for the photovoltaic output current (Ipv) at 2000w/m^2

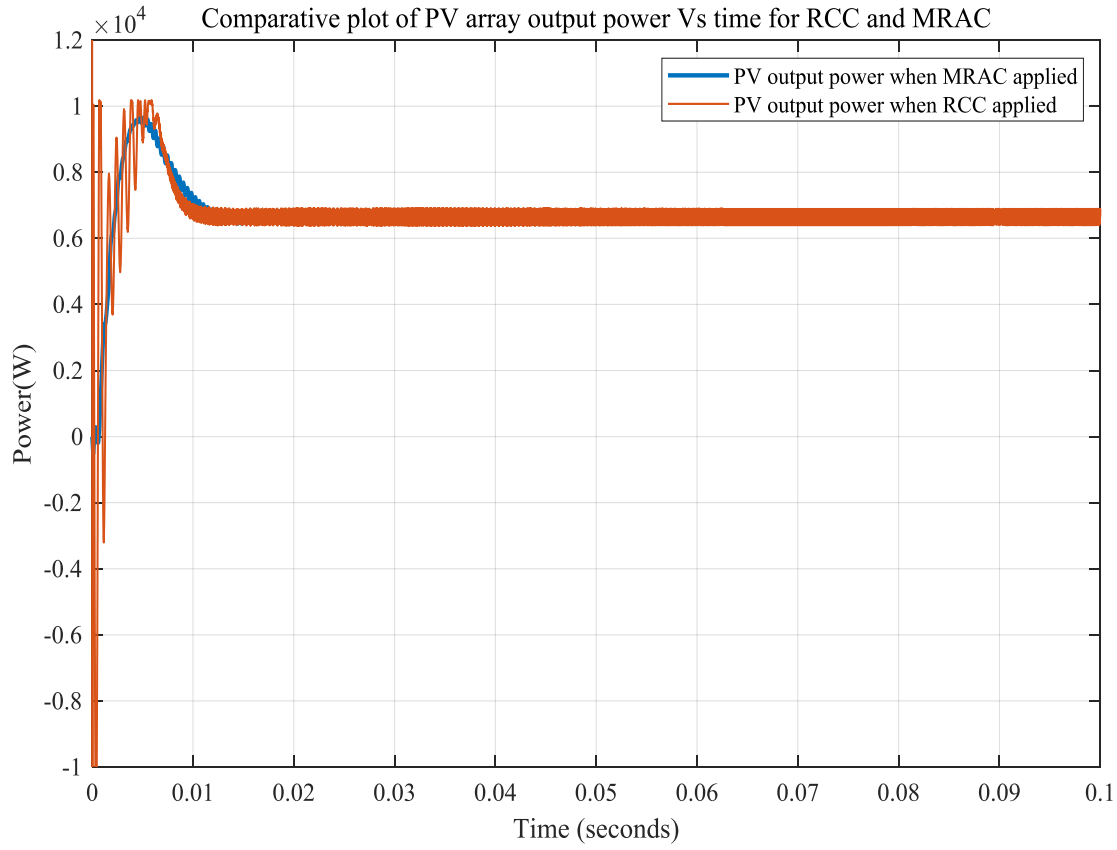

Figure 5.27: Simulation result for the photovoltaic output power (Ppv) at 2000w/m^2

From simulation results shown in figure 5.25 to figure 5.27 for irradiation level of 2000w/m^2, the proposed controller MRAC reduces the oscillation that appears when the RCC was applied. In all simulation results the settling time for the system output and overshoot were reduced.

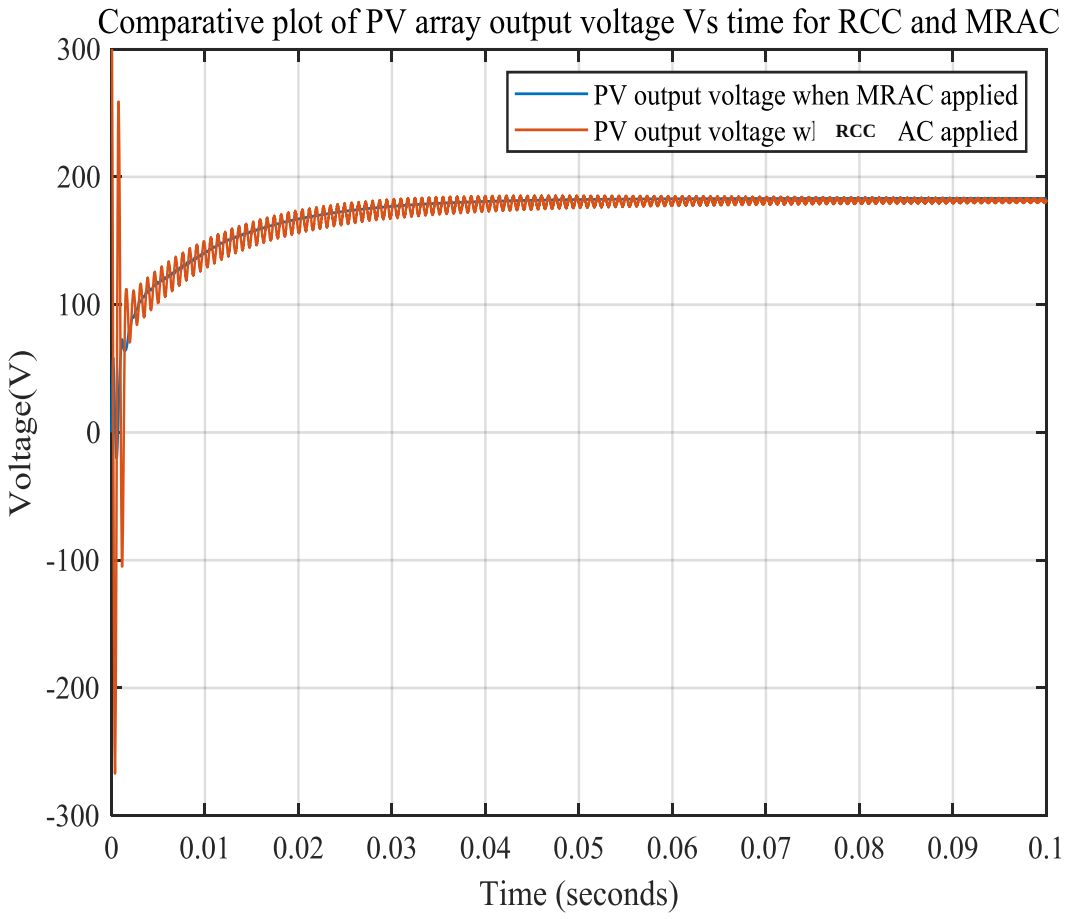

Figure 5.28: Simulation result for the photovoltaic output voltage (V_{pv}) at 800w/m^2

From the above figure 5.28 simulation result, it is observed that the photovoltaic output voltage reaches its maximum value, 181.5V and settled rapidly at t=0.05s when proposed controller, the MRAC was used. When existing controller, the RCC is used there is an oscillation at even at t=0.1s in the maximum voltage. This simulation result shows the proposed controller, MRAC reduces the oscillations that occur at the MPP and the settling time**.** In the following section the simulation was performed under varying solar irradiance conditions.

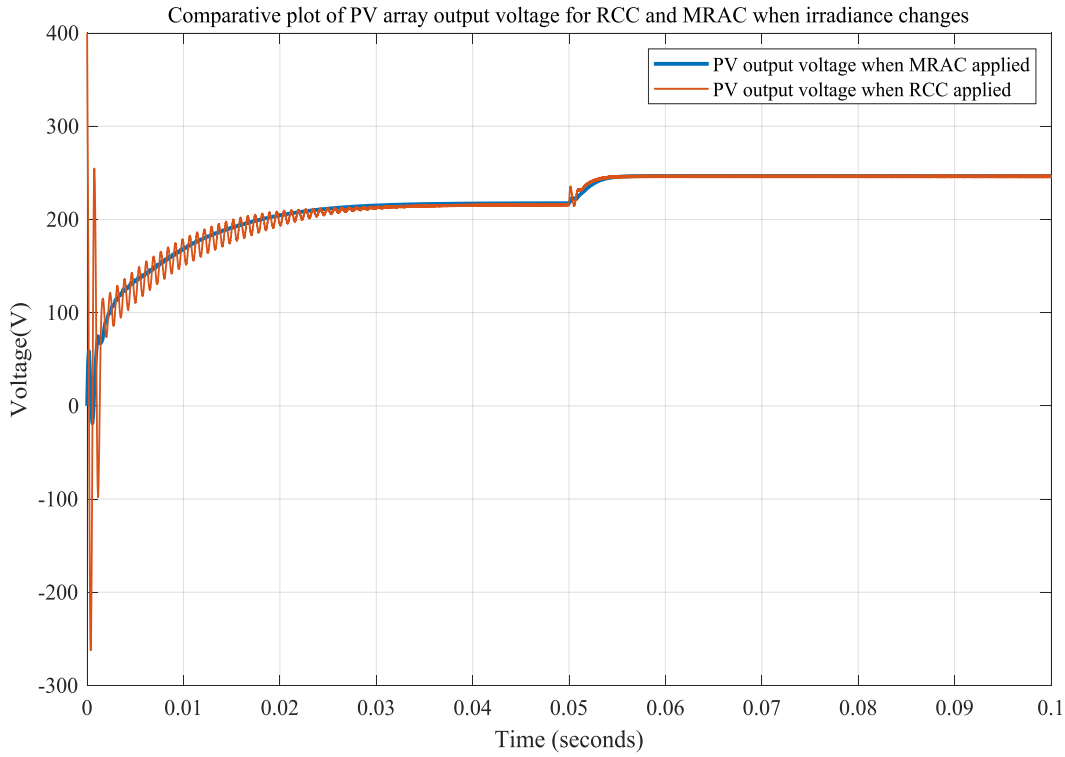

Figure 5.29: Simulation result of the photovoltaic voltage when irradiance varies from 1000 w/m^2 to 2000w/m2

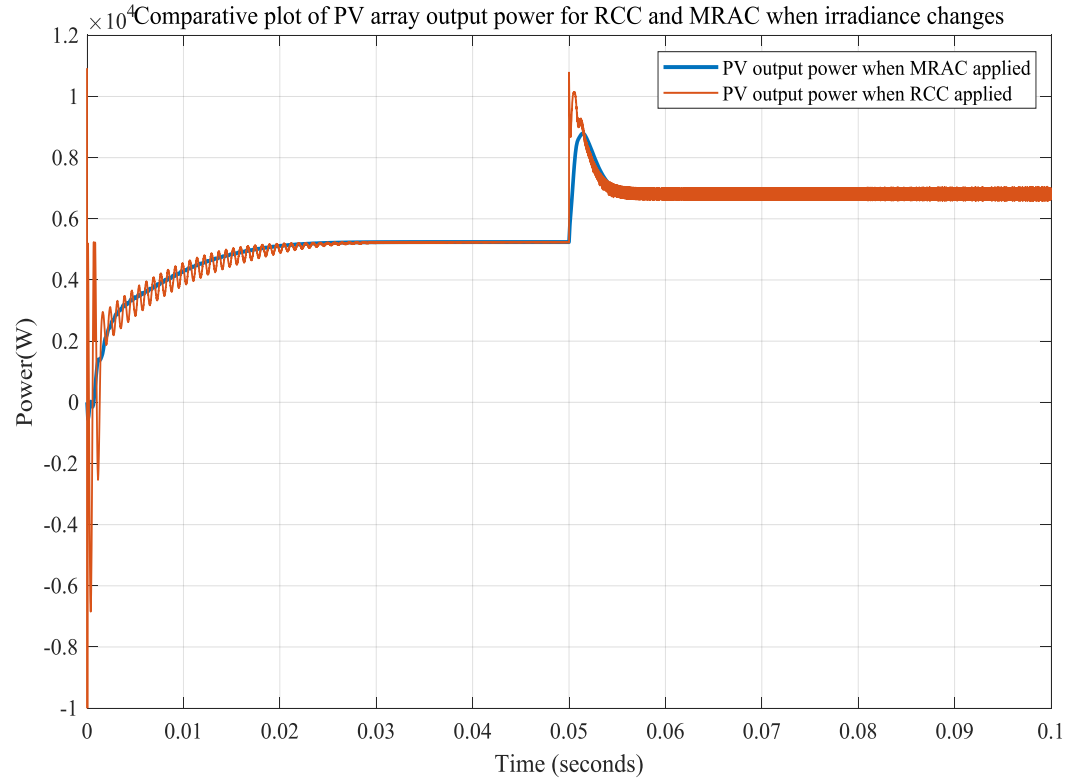

Figure 5.30: Simulation result of the photovoltaic power (Ppv) when irradiance varies from 1000w/m^2 to 2000w/m^2

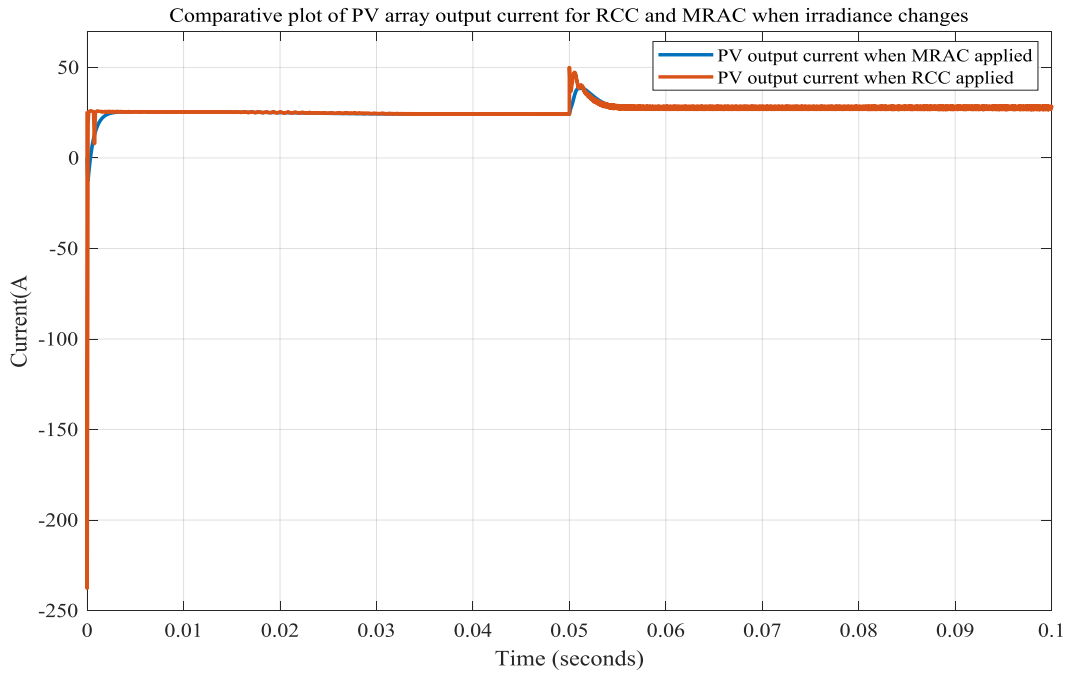

Figure 5.31: Simulation result of the photovoltaic current (I_{pv}) when irradiance varies from 1000w/m^2 to 2000w/m^2.

From the simulation result shown in figure 5.29 and figure 5.30 When the irradiation level is 1000 W/m^2 the values of the PV array voltage and power are 217 V and 5237W respectively that correspond to MPP for the irradiation level of 1000 W/m^2. The irradiation level is varied from 1000 W/m2 to 2000 W/m^2 at t=0.05s. The PV array voltage and power is settled at 248.2 V and 6887W that correspond to MPP for irradiation level of 2000 W/m2. It can be verified from both figure 5.30 and figure 5.31 that the operating point is tracking the MPP under varying irradiance condition.

Generally, as shown in Table 4.1 the proposed controller, the MRAC gives a better performance, and it is more stable than ripple correlation control. The MRAC shows good performance by reducing settling time and overshoot.

Table 5.1: Performance characteristics comparison of the RCC and the MRAC for maximum power tracking

criteria	Voltage		Power		Current	
	RCC	MRAC	RCC	MRAC	RCC	MRAC
Settling time(sec)	0.035	0.025	0.031	0.025	0.0007761	0.0005833
Maximum overshoot (%)	8.82	0.791	37.32	0.555	0.461	0.442

CHAPTER SIX
CONCLUSIONS AND RECOMMENDATIONS

6.1 Conclusions

In this thesis, the MPPT using the model reference adaptive controller for a solar power generation system was designed. Before going to the design procedure the MPPT methods, which are useful to find the MPP were revised. Then the mathematic model of the PV module, DC-DC boost converter, Ripple correlation controller and MRAC was developed. Also the system is linearized by using small-signal model since it is nonlinear. Finally, the system has been simulated with MATLAB Simulink. First, the simulations of the PV panel was done to show the characteristics voltage current (V-I)and voltage power (V-P).To show characteristics the irradiance and temperature values were varied, different values of maximum power points were observed. From these observations there is unique maximum power point for each radiation and temperature values because there is unique V_{MMP} and I_{MMP}. Secondly, the simulation of the DC-DC boost converter was done for different input voltages and duty cycles with the parameters derived earlier and satisfies the relationship between duty cycle, input voltage, and output voltage. For those parameters the system was validated. From the simulation done for boost converter it is observed that the converter boosts the input voltage in its output as desired. Thirdly, the RCC was designed. The RCC uses the product of the voltage and power ripples, which are inherent to the system, to drive the operating point towards MPP. From the simulation result it is observed that the RCC attains unique maximum power point for different irradiance level. From the observations the proposed algorithm is working satisfactorily under dynamic irradiance conditions but the main problem was observed, which is the oscillation in maximum power points. Finally, to reduce this oscillation appears in the RCC, the MRAC was designed. To design MRAC critically damped reference model and Lyapunov stability approach was used. Then results from both controllers were compared.

Generally, the simulation results show that, under proposed controller the performance characteristics of systems are greatly improved. The improvements are as follows:

- For the PV array output Voltage, the settling time and overshoot were improved by 86.04% and 66.82% respectively as compared to that obtained by using ripple correlation controller.

- For the PV array output current, settling time and overshoot were improved by 24.84% and 4.1% respectively as compared to that obtained by using the ripple correlation controller.
- For the PV array output power, settling time and overshoot were improved by 19.35% and 98.4% respectively as compared to that obtained by using ripple correlation controller.

From the Simulation results of both controllers, the settling time is short when MRAC is used. The system attains its maximum power rapidly and oscillation is reduced. Therefore, from the simulation results, we can be concluded that the performance of the system using MRAC is better and more stable than RCC.

6.2 Recommendations and Future work

Depending on the results, the proposed method improved the oscillations that exist in other MPPT algorithms. So it better to use model reference adaptive maximum power point controller other than using Maximum power point tracking controllers. As future work, the system performance can be further improved by considering multimodal characteristics of PV array and using more advanced controllers.

REFERENCES

[1] F. Eduardo, M. Berenguel, R. Fransisco and D. Matinez, Control of solar energy system, london: Springer-Verlag London Limited, 2012, pp. 1-20.

[2] G. Mircea, p. Marius-Constantin, B. Valentina and c. Doina, "Control for solar energy convertion," Proceedings of the International Conference on ENERGY and ENVIRONMENT TECHNOLOGIES and EQUIPMENT , vol. 1, no. 1790-5095, pp. 123-128.

[3] S. Lindenberg, "20% Wind Energy By 2030: Increasing Wind Energy Contribution to US," DIANE Publishing, 2009.

[4] Y. liang, z.xu, j. xia, s. tsai, y. wu and g. li, "For the bright future bulk hetero junction polymer solar cells with power conversion efficiency of 7.4%," vol. 22, pp. 2-12, 2010.

[5] A. A.R, I. Y.M., W. Leow, M. Irwanto, I. Safwati and M. Zhafarina, "Investigation of the Effect Temperature on Photovoltaic (PV) Panel Output Performanc" Centre," vol. 6, no. 5, 2016.

[6] [Online]. Available: http://www.alternative energy tutorials.com/solar cells I-V characteristics.html. [Accessed 19 05 2019].

[7] K. M, Bataineh and H. Amr, "Efficient Maximum Power Point Tracking Algorithm for PV Application under Rapid Changing Weather Condition," vol. 1, pp. 5-12, 2014.

[8] N. Byamakesh, A. Mohapatra and K. B. Mohanty, "Selection criteria of dc-dc converter and control variable for MPPT of PV system utilized in heating and cooking applications," Electrical & Electronic Engineering research article, vol. 1, pp. 3-10, 2017.

[9] R. Hegazy and M. E. Ali, "A comprehensive comparison of different MPPT techniques for photovoltaic systems," ScienceDirect, pp. 3-13, 2014.

[10] S. M. David, "Maximum Power Point Tracking Algorithms for Photovoltaic Applications," no. 14, pp. 3-7, 2010.

[11] S. Sumedha, "Maximum Power Point Tracking Algorithms for Photovoltaic System," International Review of Applied Engineering Research, vol. 4, pp. 147-154, 2014.

[12] R. Faranda and S. Leva, "Energy comparison of MPPT techniques for PV Systems," no. 6, 2008.

[13] T. Esram, J. W. Kimball, P. T. Krein, P. L. Chapman and P. Midya, "Dynamic Maximum Power Point Tracking of Photovoltaic Arrays Using Ripple Correlation Control," IEEE transactions on power electronics, vol. 21, no. 5, pp. 5-9, 2006.

[14] A. Trivedil, A. Gupta, R. K. Pachauri and Y. K. Chauhan, "Comparison of Perturb & Observe and Ripple Correlation Control MPPT Algorithms for PV array," Electrical Engineering Department, School of Engineering,Gautam Buddha University, Greater Noida, India., 2016.

[15] R. B, A. Koad and A. F. Zobaa, "Comparative study of five maximum power point tracking techniques for photovoltaic systems," Brunel University, London, United Kingdom , pp. 1-9.

[16] F. Kazan, S. Karaki, R. A. Jabr and M. Mansour, "Maximum Power Point Tracking Using Ripple Correlation and Incremental Conductance," IEEE, pp. 3-12, 2012.

[17] A. Hafte, "Design of Lyapunov rule based model reference adaptive control with decoupler with fpr boiler-turbine-generator," addis ababa university, 2019.

[18] P. H. a. K. B. A. William S. Black 1, "Adaptive Systems: History, Techniques, Problems,and perspectives," systems, vol. 2, pp. 1-55, 2014.

[19] K. J. Astrom and B. W. mark, Adaptive control, Pearson education, 2001.

[20] J. M. Lemos, Adaptive Control of Distributed Collector Solar Fields, vol. 37, International Journal of Systems Science, 2006.

[21] F. Jaramillo and G. K. Lopez, "Adaptive control scheme for grid connected photovoltaic systems with unknown bounds," no. 7, pp. 1-9, 2004.

[22] L. Piegari, R. Rizz, I. Spina and P. Tricoli, "Optimized Adaptive Perturb and Observe Maximum Power Point Tracking Control for Photovoltaic Generation," pp. 1-8, 2015.

[23] A. K. Abdelsalam, A. M. Massoud, S. Ahmed and P. N. Enjeti, "High Performance Adaptive Perturb and Observe MPPT Technique for Photovoltaic-Based Microgrids," IEEE Transactions on power electronics, vol. 26, no. 4, pp. 3-7, 2011.

[24] R. R. I. S. P. T. Luigi Piegari, "Optimized Adaptive Perturb and Observe Maximum Power Point Tracking control for photovoltaic generation," Energies, no. 27, pp. pp 1-19, 2015.

[25] C. L. S. S. S. E. S. Satish R, "A Maximum Power Point Tracking Technique baesd on ripple correlation control for single phase single stage grid connected photovoltaic system," National Institute of Technology Goa, India., pp. 1-5, 2016.

[26] K. S. N. Vyshnavi, "Model Reference Adaptive Control for Maximum Power Point Tracking in PV system," IJARIIE, vol. 1, no. 5, 2015.

[27] Kanimozhi.G, Meenakishi.J and Sreedevi.VT, "Small signal modeling of a DC-DC type double boost converter integrated with SEPIC converter using state space averaging approach," VIT university, vandalur-kelambakam road Chennai-600127,india.

[28] M. F. Borja, "Dynamic modelling of a DC to DC boost converter," no. 1, pp. 1-5.

[29] D. S. Morales, "Maximum Power Point Tracking Algorithms for Photovoltaic Applications," Aalto University,Faculty of Electronics, Communications and Automation, pp. 3-55, 2010.

[30] A. K. Mahammad, S. Saon and W. S. Chee, "Development of Optimum Controller based on MPPT for Photovoltaic System during Shading Condition," Procedia Engineering, no. 53, p. 337 – 346, 2013.

[31] D. Singh, RiaYadav and Jyotsana, "Perturb and Observe Method MATLAB Simulink and Design of PV System Using Buck Boost Converter," International Journal of Science Engineering and Technology Research (IJSETR), vol. 3, no. 6, pp. 3-12, 2016.

APPENDIX

Appendix A. Algorithim of perturb and obseve(P&O).